

Iron(III)-induced activation of chloride from artificial sea-salt aerosol

Julian Wittmer,^{A,D} Sergej Bleicher,^{A,B} Johannes Ofner^C and Cornelius Zetzsch^A

^AAtmospheric Chemistry Research Unit, Bayreuth Center of Ecology and Environmental Research (BayCEER), University of Bayreuth, Dr Hans-Frisch Strasse 1–3, D-95448 Bayreuth, Germany.

^BDepartment of Forensic Toxicology, Synlab MVZ Weiden GmbH, Zur Kesselschmiede 4, D-92637 Weiden, Germany.

^CDivision Environmental and Process Analytics, Institute of Chemical Technologies and Analytics, Vienna University of Technology, AT-1060 Vienna, Austria.

^DCorresponding author. Email: julian.wittmer@uni-bayreuth.de

Environmental context. Inorganic, natural aerosols (sea-salt, mineral dust, glacial flour) and contributions of anthropogenic components (fly ash, dust from steel production and processing, etc.) contain iron that can be dissolved as Fe^{III} in saline media. This study investigates photochemical processes in clouds and aerosols producing gas-phase Cl as a function of salt- and gas-phase composition employing a simulation chamber. Atomic Cl may contribute to the oxidative capacity of the troposphere, and our findings imply local sources.

Abstract. Artificial sea-salt aerosol, containing Fe^{III} at various compositions, was investigated in a simulation chamber (made of Teflon) for the influence of pH and of the tropospheric trace gases NO₂, O₃ and SO₂ on the photochemical activation of chloride. Atomic chlorine (Cl) was detected in the gas phase and quantified by the radical clock technique. Dilute brines with known Fe^{III} content were nebulised until the relative humidity reached 70–90%. The resulting droplets (most abundant particle diameter: 0.35–0.46 μm, initial surface area: up to 3 × 10⁻² cm² cm⁻³) were irradiated with simulated sunlight, and the consumption of a test mixture of hydrocarbons was evaluated for Cl, Br and OH. The initial rate of atomic Cl production per aerosol surface increased with Fe^{III} and was ~1.9 × 10¹⁸ atoms cm⁻² s⁻¹ at Cl⁻/Fe^{III} = 13. The presence of NO₂ (~20 ppb) increased it to ~7 × 10¹⁸ atoms cm⁻² s⁻¹, the presence of O₃ (630 ppb) to ~9 × 10¹⁸ atoms cm⁻² s⁻¹ and the presence of SO₂ at 20 and 200 ppb inhibited the release slightly to ~1.7 and ~1.1 × 10¹⁸ atoms cm⁻² s⁻¹. The observed production of atomic Cl is discussed with respect to pH and speciation of the photolabile aqueous Fe^{III} complexes.

Received 20 December 2014, accepted 27 March 2015, published online 2 July 2015

Introduction

Iron-containing aerosols have natural (e.g. mineral dust, glacial flour) or anthropogenic (combustion of fossil fuel, fuel-oil fly ash, metal processing industry, etc.) sources and represent (together with upwelling) the source of dissolved iron in off-shore waters.^[1] The deposited dissolved iron, in the range of 0.26 Tg year⁻¹,^[2] has been suggested as being coupled to atmospheric carbon dioxide (CO₂) concentration by activation of the oceanic food chain ('Iron hypothesis').^[3–7] Apart from fertilisation of the oceans, iron is known to act as a catalyst in the photo-Fenton cycle in ferrous (Fe²⁺) and ferric (Fe³⁺) form, and it is utilised in wastewater treatment. Concerning the role of iron in the atmosphere, besides the proposed indirect CO₂ reduction, the interactions between gaseous and aqueous phases containing iron and other organic and inorganic compounds are of interest.

Reactive halogen species (RHS) have a large effect on the budget of ozone (O₃) and nitrogen oxides (NO_x), affecting the oxidation capacity of the atmosphere^[8,9] and interacting with secondary organic aerosols.^[10] In particular, the atomic chlorine radical (Cl) is an important atmospheric oxidant that can considerably influence the lifetime of methane (CH₄).^[11] The main mechanisms responsible for the activation of halides

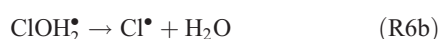
to reactive forms are well investigated, including heterogeneous activation by NO_x and O₃ and autocatalytic halogen activation by HOBr and HOCl.^[12,13] However, the potential role of iron in the release mechanisms of RHS remains unclear and is of special interest in the current work. Whereas a global tropospheric influence is questionable, the photochemistry of iron can significantly contribute to atomic Cl production in the gas phase, at least in some regions. Relevant iron–halide mixtures are present e.g. in coastal regions, intertidal zones, the combustion plumes of ships, volcanic plumes or brine-containing soils. In particular, hypersaline environments, such as the Dead Sea or Australian salt lakes,^[14] offer conditions that promote iron-induced halogen release, as recently investigated by Wittmer et al. for modelled salt surfaces.^[15] The present study, however, concentrates on the effect of Fe³⁺ in saline aerosols that can also be found in these regions and when mineral aerosol particles mix with sea salt. In particular, chloride (Cl⁻) enhances the dissolution of iron.^[16] The dominant presence of dissolved Fe³⁺ in saline aerosols and the photoreduction to Fe²⁺ were observed by several studies,^[17–19] but mainly with a focus on the role of the photochemistry of iron in the aqueous phase.^[20] Whereas the photolysis of ferric ions in saline media has been well

investigated,^[21–23] less effort has been directed at the implications for the gas phase.

The photolysis of FeCl_2^{2+} and FeCl_2^+ directly yields chlorine atoms (Cl^\bullet) in the liquid phase of the humid saline aerosol, and these react very fast with Cl^- to form $\text{Cl}_2^{\bullet-}$ (R1, reaction rate constant $k = 2 \times 10^{10} \text{ M}^{-1} \text{ s}^{-1}$ ^[21]). For convenience, only aqueous-phase radicals will be marked with a dot in the following. The combination of Cl^\bullet with another $\text{Cl}_2^{\bullet-}$ (R2), or alternatively the combination of two $\text{Cl}_2^{\bullet-}$ (R3) and the dissociation of the produced Cl_3^- thereby (R4) leads to a degassing of Cl_2 .^[24]



An alternative, indirect pathway for chloride activation is the photolysis of the slightly less photoactive species FeOH^{2+} , producing OH^\bullet radicals in the liquid that again can form Cl^\bullet by $\text{ClOH}^{\bullet-}$.



A more detailed summary and description of Fe^{III} -induced Cl_2 formation can be found in Lim et al.^[24] or Wittmer et al.^[15]

In addition to the photosensitive iron-induced halogen release mechanism, further trace gas species, such as O_3 , NO_x and sulfur dioxide (SO_2), possibly influence Cl_2 release, mainly when dissolved in the aqueous phase where they can change the pH,^[25] coordinate with Fe^{2+} or Fe^{3+} ,^[26] scavenge Cl^\bullet ^[22] or additionally activate halides by the known heterogeneous mechanisms.^[13] Concerning O_3 , Sadanaga et al.^[27] observed an enhancement of the O_3 uptake rate and Cl_2 release in the presence of water-soluble Fe^{3+} and O_3 in the dark. When SO_2 is involved, the absorbed amount is highly pH-dependent.^[28] The dissolved SO_2 is mainly in bisulfite and sulfite forms, which are oxidised to sulfate depending on the pH and the availability of catalysts such as Fe^{3+} .^[29,30] The presence of sulfate can strongly inhibit the chloride activation process by scavenging Cl^\bullet and OH^\bullet or forming stable complexes with ferrous ions.^[15,22] Apart from iron-influenced systems, polluted air masses considerably influence halogen activation in sea salt,^[8,12,31,32] as well as the environmental oxidation of Cl^- and Br^- by the triplet states of chromophoric dissolved organic matter.^[33] The present study aims at a deeper insight into the effects of Fe^{III} in saline media with a focus on a better quantification of surface-related gaseous Cl production and the effects of the trace gases mentioned above.

Experimental

Smog-chamber set-up

The experiments were conducted in a cylindrical Teflon smog chamber (fluorinated ethylene propylene, FEP 200A, DuPont, Wilmington, DE, USA) with a volume of more than 3500 L (diameter: 1.33 m, height: 2.5 m, surface/volume ratio: 3.8 m^{-1}). Here, the chamber and its analytical instrumentation

are only briefly introduced. More detailed specifications can be found elsewhere.^[15,31,34]

The chamber was suspended above a solar simulator that generates a mean actinic flux comparable with the summer sun at 50° latitude. The chamber was equipped with a differential pressure sensor (Kalinsky Elektronik DS1, Kalinsky Sensor Elektronik GmbH & Co. KG, Erfurt, Germany) to monitor the slight overpressure of 0.6–1 Pa, which was controlled by a continuous flow of 5–6 L min^{-1} of hydrocarbon-free, humidified zero air (zero-air generator, cmc instruments, <1 ppb of O_3 , <500 ppt NO_x , <100 ppb of CH_4) for all experiments. The temperature was adjusted to 20°C and monitored by two light-shielded sensors (Rotronic, HC2-IC102) at different heights (bottom and top) to observe and avoid possible thermic layering. A Teflon fan inside the chamber assured constant mixing and kept temperature gradients below 1°C . NO , NO_x and O_3 were monitored by chemiluminescence gas analysers (EcoPhysics, CLD 88p (EcoPhysics GmbH, Dürnten, Switzerland) coupled with a photolytic converter, PLC 860, for NO and NO_x , and UPK 8001 (Bendix, Bad Nauheim, Germany) for O_3).

Gas-phase Cl , Br and OH were indirectly quantified by the radical clock method,^[35] monitoring the consumption of selected hydrocarbons (2,2-dimethylpropane, DMP, Linde AG, Munich, Germany, $\geq 99\%$; 2,2-dimethylbutane, DMB, Sigma-Aldrich Chemie GmbH, Taufkirchen, Germany, $\geq 99\%$; 2,2,4-trimethylpentane, TMP, Janssen-Cilag GmbH, Neuss, Germany, $\geq 99\%$; toluene, Tol, Aldrich $\geq 99.9\%$) and *n*-perfluorohexane (PFH, Aldrich, $\geq 99\%$) as inert standard. The concentrations of the hydrocarbons was measured at time intervals of 15 min by gas chromatography (GC, Siemens Schromat 2, 50-m Al_2O_3 -PLOT column, 0.25 mL min^{-1} He as carrier gas) with a flame ionisation detector (FID), custom-built liquid nitrogen cryo-trap enrichment in glass-lined stainless-steel tubing and a Nafion tube counterflushed from outside with zero air to dry the sampling flux.^[15]

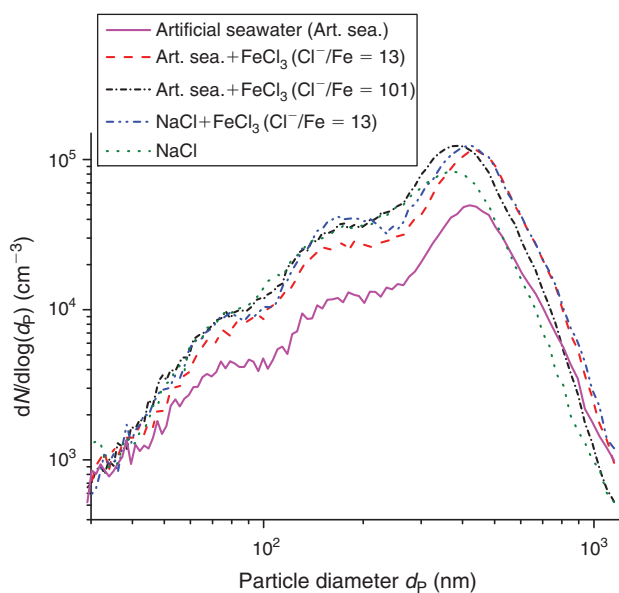
Sample preparation and chemicals used

An artificial seawater stock solution with a molar Cl^-/Br^- ratio of 997 was prepared according to Kester et al.^[36] The mixture included NaCl (23.9 g L^{-1}), $\text{Na}_2\text{SO}_4 \cdot 10\text{H}_2\text{O}$ (9.1 g L^{-1}), KCl (0.68 g L^{-1}), NaHCO_3 (0.2 g L^{-1}), KBr (0.098 g L^{-1}), H_3BO_3 (0.026 g L^{-1}), NaF (0.003 g L^{-1}), MgCl_2 (5.1 g L^{-1}), and $\text{CaCl}_2 \cdot 2\text{H}_2\text{O}$ (1.5 g L^{-1}). Depending on the experiment, a specific amount of FeCl_3 was dissolved in the stock solution and diluted afterwards (1:28) to obtain a Cl^- concentration of 15–35 mmol L^{-1} (Table 1) that provides optimal aerosol size distributions for long residence times of the suspended droplets. The aerosol production from the prepared solutions and the subsequent measurement are described in the following section. For the reference experiment with Fe^{III} -doped NaCl , the FeCl_3 was directly added to an 18 mmol L^{-1} NaCl solution. The added amount of FeCl_3 and the resulting $\text{Cl}^-/\text{Fe}^{\text{III}}$ ratios are listed in Table 1. More details of the prepared artificial seawater are included in the Supplementary material (Table S1).

On the basis of the different sea-salt mixtures, the effect of various gas species was tested by adding O_3 from a silent ozoniser (Sorbios GSG 12, Sorbios GmbH, Berlin, Germany) with an electrical discharge applied to pure oxygen (Rießner-Gase GmbH, Lichtenfels, Germany, $>99.995\%$), NO_2 from a gas cylinder (Rießner Gase, 104 vpm (volume parts per million) NO_2 with a purity of 98% in synthetic air), or SO_2 from a gas cylinder (Rießner Gase, 0.99% SO_2 with a purity of 99.98% in N_2 with a purity of 99.999%).

Table 1. Compositions of the stock solutions obtained by adding FeCl₃ to the artificial seawater (prepared according to Kester et al.^[36]) or to a 1 g L⁻¹ NaCl solution and resulting molar Cl⁻/Fe^{III} ratios

Manufacturer and specified purity (%)	Amount weighted in 1 L H ₂ O (g)	Cl ⁻ /Fe ³⁺ (mol mol ⁻¹)	Cl ⁻ concentration in the nebulised solution (mmol L ⁻¹)
Added FeCl ₃ to artificial seawater			
Merck, for synthesis, ≥98 %	0.14	955	28
Merck, for synthesis, ≥98 %	1.36	101	29
Riedel de Haën, sublimated, ≥99 %	2.67	53	30
Riedel de Haën, sublimated, ≥99 %	13.04	13	37
FeCl ₃ added to 1 g L ⁻¹ NaCl			
Riedel de Haën, sublimated, ≥99 %	0.278	13	18

**Fig. 1.** Typical initial (multiple-charge-corrected) size distributions for aerosols generated by the ultrasonic nebuliser (30–50-min injection time) from various diluted stock solutions containing NaCl, FeCl₃ or artificial seawater. N , number density; d_p , particle diameter.

Aerosol production and measurement

The sea-salt particles were generated by nebulising the prepared solutions (Table 1) with an ultrasonic nebuliser (Quick Ohm QUV-HEV FT25/16-A, 35 W, 1.63 MHz, Quick-Ohm Küpper & Co. GmbH, Wuppertal, Germany) at a starting relative humidity (RH) of ≥40 % to avoid crystallisation.^[12] During injection (taking typically 30–50 min), the RH increased to 70–90 %. Thus, we can assume that the droplets equilibrate to form a saturated solution, leading to most abundant particle diameters between 350 and 460 nm based on the concentration of the stock solution and the final RH after injection.^[37] The size distributions were determined by an electrostatic classifier (TSI, 3071, TSI GmbH, Aachen, Germany) in combination with a neutraliser (⁸⁵Kr) and a condensation nucleus counter (TSI, 3020). The scanning method and the multiple charge correction were applied with custom-written software.^[38] Typical size distributions, determined after 30–50 min of injection, are shown in Fig. 1 for different stock compositions. To avoid the condensation of the sea salt within the transfer line (~6.4-mm tube made of copper) and thus the dripping of solution inside the chamber, the tube was additionally heated by a heating wire to ~60–70 °C.

During aerosol generation, the NO_x signal rose typically up to 3–5 ppb, probably originating from the sonochemical formation of nitrate and nitrite^[39] and including a possible cross-sensitivity of the NO_x analyser to nitrous acid (HONO).^[40]

The chamber walls were either cleaned with deionised water (Seralpur Pro 90 CN, <0.055 μS cm⁻¹, Seral, Ransbach-Baumbach, Germany), or the total FEP-Teflon film was exchanged after the experiment (depending on the risk of contamination expected for subsequent runs). To minimise the outgassing of gas-phase products,^[41] every new chamber was conditioned by adding O₃ at an RH of 50–80 % and irradiating for at least 4 h with the solar simulator and an additional UV lamp (Phillips TUV 55 W, λ = 253.7 nm).

After every experiment, the particles were collected by a Sioutas cascade impactor (SKC) in the aerodynamic diameter ranges of >2.5, 1–2.5, 0.5–1, 0.25–0.5 and <0.25 μm^[42] on aluminium foil as a collection substrate. The impactor samples were analysed using an FEI Quanta 200 scanning-electron microscope (SEM), equipped with an energy-dispersive X-ray (EDX) detector for imaging (Octane Pro Silicon Drift (SDD) EDX detector from AMETEK GmbH, Wiesbaden, Germany). The hyperspectral data-cube from the SEM-EDX measurements was analysed using the software package *Imagelab* (Epina Software Laboratories, www.imagelab.at, accessed April 2015).^[43]

Data analysis (radical clock)

The gas chromatograms were evaluated the same way as described before^[15] to quantify the quasi-stationary concentrations of Cl_{qs}, OH_{qs}, and Br_{qs} in the gas phase, based on the measured, dilution-corrected and smoothed hydrocarbon (HC_{*i*}) profiles, resulting in a system of four differential equations with three unknown variables according to:

$$-\frac{d\ln[\text{HC}_i]}{dt} = k_{\text{Cl},i}[\text{Cl}] + k_{\text{Br},i}[\text{Br}] + k_{\text{OH},i}[\text{OH}] \quad (1)$$

where $k_{X,i}$ is the reaction rate constant of HC_{*i*} towards the radical X (X = Cl, Br, and OH; Table S2, Supplementary material). The corresponding total production (Q_X) and production rates (dQ_X/dt) are obtained by equalising sources and sinks in a photostationary steady-state:

$$Q_X = \int_0^\tau \sum_i k_{X,i}[\text{HC}_i]_t[\text{X}]_t dt \quad (2)$$

Considering a constant total reactivity of the chamber contents towards [X] on the one hand ($\sum_i k_{X,i}[\text{HC}_i]_0$) and only the reactivity

of the measured hydrocarbons on the other hand ($\sum k_{X,i}[\text{HC}_i]$), which means either assuming that reaction products have the same reactivities as the HC_i or neglecting the reactivities of the reaction products totally, we obtain an estimate of the minimum and maximum Q_X and dQ_X/dt . These assumptions are reasonably valid for Cl atoms but less reliable for Br atoms and OH radicals, where the reactivities of reaction products may exceed the reactivities of the original hydrocarbons by far. However, they are valid at the very beginning of the irradiation, where the consumption of the hydrocarbons is still low.

The measurements of the particle size distributions (number density N , cm^{-3}) allow us to determine the available reaction surface area (A , $\text{m}^2 \text{m}^{-3}$) and the particle volume (V_{particle} , $\text{m}^3 \text{m}^{-3}$), which equals the liquid water content (LWC) plus the tare volume of the ions (radius, $r_{\text{Cl}^-} = 181$ pm, $r_{\text{SO}_4^{2-}} = 230$ pm, $r_{\text{Na}^+} = 102$ pm, $r_{\text{K}^+} = 138$ pm, $r_{\text{Mg}^{2+}} = 72$ pm, $r_{\text{Ca}^{2+}} = 100$ pm, $r_{\text{Fe}^{3+}} = 65$ pm)^[44] at the adjusted RH. The measured LWC was corrected by considering the main ions as spherical. The contribution of deposited particles on the chamber walls to the activated Cl was considered by measuring the Cl activation of a totally wall-deposited aerosol load (*Chamber wall effects* section). The Cl^- production terms are normalised to obtain absolute production rates, dQ_{abs}/dt , and absolute total production Q_{abs} cm^{-2} of the aerosol surface. Therefore, the production rate (atoms $\text{cm}^{-3} \text{s}^{-1}$) is multiplied by the chamber volume (V_{chamber}) to obtain the total number of atoms produced per second. The result is divided by the actual active aerosol surface, which we define as the sum of (i) the measured aerosol surface when the lights were turned on ($A_{0,\text{light}}$) and its deposition rate, $\exp(-t_{\text{light}}/\tau_S)$, with the aerosol surface lifetime τ_S ; (ii) the active, deposited surface during the time of injection; and

(iii) the active, deposited surface formed after the injection is finished (Eqn 3). Whereas (ii) is determined by assuming an approximately linear increase of the aerosol surface during injection and calculating the respective deposition until the injection is stopped ($t_{\text{inj, end}}$), (iii) is based on the measured aerosol surface area directly after injection ($A_{0,\text{inj}}$) and its deposition during the time t_{inj} , which starts when the injection ends. Both terms are multiplied by a factor of 0.2, which is the fraction of deposited surface area that contributes to the halogen activation (*Chamber wall effects* section).

$$\frac{dQ_{\text{abs}}}{dt_{\text{light}}} = \frac{\frac{dQ_X}{dt_{\text{light}}} \times V_{\text{Chamber}}}{A_{0,\text{light}} \times \exp\left(-\frac{t_{\text{light}}}{\tau_S}\right) + 0.2 \times \left(\int_{t_{\text{inj, start}}}^{t_{\text{inj, end}}} \left(\frac{\Delta A_{0,\text{inj}}}{\Delta t_{\text{inj, end}}} \times \frac{t}{\tau_S} \right) dt + A_{0,\text{inj}} \times \left(1 - \exp\left(-\frac{t_{\text{inj}}}{\tau_S}\right) \right) \right)} \quad (3)$$

Results and discussion

Table 2 presents an overview of the experiments performed, including $\text{Cl}^-/\text{Fe}^{\text{III}}$ ratios, pH of the diluted stock solution, gas-phase composition, initial reactivity of HCs against Cl, OH, and Br, initial aerosol surface, resulting quasi-stationary concentrations and absolute production. Based on the two-to-five orders of magnitude lower reactivity of the applied HCs against Br and OH compared with Cl, depletion was dominated by the reaction with Cl, and no significant interpretation for Br and OH was possible in most cases. Before adding FeCl_3 to the samples,

Table 2. Molar $\text{Cl}^-/\text{Fe}^{\text{III}}$ ratio, pH of the diluted, nebulised stock solution, gas-phase composition within the smog chamber, total initial reactivity of the hydrocarbons in the chamber against Cl, OH and B, total aerosol surface measured directly after injection, quasi-stationary Cl_{qs} , Br_{qs} and OH_{qs} concentrations during irradiation during the first hour, and resulting total Cl and Br production per square centimetre aerosol surface
n.d., not detected

$\text{Cl}^-/\text{Fe}^{3+}$	pH of diluted stock solution	Gas phase	Initial reactivity (s^{-1})			Initial aerosol surface area ($10^{-2} \text{m}^2 \text{m}^{-3}$)	Quasi-stationary concentration (atoms cm^{-3})			Total production Q_{abs} (atoms $\text{cm}^{-2} \text{h}^{-1}$)	
			Cl	OH	Br		$\text{Cl}_{\text{qs}} (\times 10^5)$	$\text{OH}_{\text{qs}} (\times 10^6)$	$\text{Br}_{\text{qs}} (\times 10^9)$	Cl ($\times 10^{21}$)	Br ($\times 10^{21}$)
∞^{A}	4.7–5.0	Zero air	182	4.5	0.0074	1.0	$\sim 0.1^{\text{F}}$	$\sim 1^{\text{F}}$	$\sim 1^{\text{F}}$	$\sim 0.3\text{--}0.4^{\text{F}}$	n.d. ^G
∞^{B}	4.8–5.1	Zero air	163	3.9	0.0063	2.3	~ 0.4	5.1	$< 1^{\text{G}}$	~ 0.6	n.d. ^G
∞^{A}	4.7–5.0	20 ppb NO_x	209	4.2	0.008	2.4	$\sim 0.1^{\text{F}}$	2	1.2	n.d. ^G	0.6–0.7
∞^{A}	4.7–5.0	700 ppb O_3	137	1.3	0.0053	2.2	4.9	17	9.4	3.1–4.9	1.6–2.8
955 ^C	4.5–4.8	Zero air	126	2.6	0.0039	1.2	$\sim 0.1^{\text{F}}$	2.3	$\sim 1^{\text{F}}$	$\sim 0.3\text{--}0.4^{\text{F}}$	n.d. ^G
101 ^C	3.9–4.2	Zero air	201	4.3	0.0077	2.5	0.5	1.2	3.8	0.7–0.8	1.8–2.0
101 ^{C,D}	2.1–2.3	Zero air	177	3.3	0.0046	1.8	1.9	2.2	2.7	5.3–5.8	1.8–2.2
101 ^C	3.9–4.2	20 ppb NO_x	196	3.9	0.0057	2.3	9.1	5	3	3.0–3.3	2.6–3.2
101 ^{C,D}	2.1–2.3	20 ppb NO_x	169	3.6	0.0053	2.3	5.4	3	$< 1^{\text{G}}$	6.8–7.9	n.d. ^G
51 ^C	3.3–3.6	Zero air	152	3.3	0.0052	3.2	1.9	5.4	1.2	1.4–1.5	~ 0.3
13 ^B	1.9–2.2	Zero air	118	2.9		2.4	16.7	4.8	$< 1^{\text{G}}$	8.7–13	n.d. ^G
13 ^C	1.9–2.2	Zero air	125	2.4	0.0036	3.0	13.1	$< 1^{\text{G}}$	$< 1^{\text{G}}$	6.6–8.7	n.d. ^G
13 ^C	1.9–2.2	20 ppb NO_x	139	3.2	0.0051	3.1	65.1	$< 1^{\text{G}}$	$< 1^{\text{G}}$	16–52	n.d. ^G
13 ^C	1.9–2.2	630 ppb O_3	218	5.2	0.0085	3.4	40	13	13	18–45	3.0–8.1
13 ^C	1.9–2.2	~ 20 ppb SO_2	204	4.9	0.0078	1.9	4.3	2.1	3.7	6.0–6.7	2.0–2.2
13 ^C	1.9–2.2	> 200 ppb SO_2	178	4.4	0.0063	1.0	1.4	1.3	1.2	4.0–4.5	1.4–1.6

^A Fe^{III} -free artificial seawater stock solution.

^BNaCl stock solution.

^CArtificial seawater stock solution.

^DpH adjusted to 2.1–2.3.

^EMean steady-state concentrations during the first hour.

^FClose to the detection limit.

^GBelow the detection limit.

several Fe^{III}-free blank experiments were performed, including pure NaCl aerosol, artificial sea-salt aerosol and artificial sea-salt aerosol with O₃ and NO₂ addition respectively (see Table 2). Except for the artificial sea-salt aerosol with addition of 700 ppb O₃, Cl production was hardly detectable. Generally, no indication of Cl, Br or OH production was observed during the dark phases (aerosol, NO₂, O₃, SO₂ injections and waiting periods), based on the constant HC time profiles.

Chamber wall effects

Owing to flashovers in the classifier throughout some experiments caused by the high RH, only the measurements at the beginning of those experiments were evaluable. Therefore, the measurements after injection and when the lights were turned on were used to calculate the dilution-corrected loss by deposition, based on the mean dilution-corrected lifetimes $\tau_{N,S}$ (N , number density; S , total aerosol surface area) over the experiments without flashovers and neglecting the loss by coagulation. The deposition velocity depends on the salt concentration in the nebulised solution and thus on the mean particle diameter after injection. For instance, the artificial sea-salt solution and the pure NaCl solution gave lifetimes of $\tau_N = 24\,800$ s ($\tau_S = 30\,100$ s) and $\tau_N = 25\,000$ s ($\tau_S = 31\,100$ s). For the higher-concentration Fe^{III}-doped artificial seawater (29–35 mmol Cl⁻ L⁻¹), the most abundant particle diameters were between 430 and 460 nm, resulting in a faster sedimentation with $\tau_N = 4590 \pm 240$ s and $\tau_S = 6070 \pm 520$ s compared with $\tau_N = 6845$ s and $\tau_S = 8820$ s for the lower-concentration pure NaCl + FeCl₃ solution (24 mmol Cl⁻ L⁻¹) with most abundant particle diameters between 390 and 420 nm. The respective contour plots can be found in the Supplementary material (Fig. S1).

To quantify the particle deposition and its contribution to the active surface area (and thus to Cl activation), a test measurement was performed to determine the fraction of Cl release by the active wall surface compared with the active aerosol surface: the iron-doped artificial seawater sample (Cl⁻/Fe^{III} = 13) was injected and allowed to deposit totally for 17 h (<0.005 % of the

surface area should have remained suspended) while keeping the RH at 80 %. Then the ‘aerosol-free’ chamber was irradiated, resulting in Cl production that was 20 ± 4 % compared with the actual production measured for the same sample in an aerosol experiment (*Iron(III)-catalysed Cl atom production* section). This production was evaluated by taking the mean of the quotient of each total production (deposited and not deposited) normalised by the respective initial LWC directly after injection. In Eqn 3, the contribution of deposited, active aerosol surface area is accounted for by adding 20 % of the deposited surface area since the time of injection to the surface area when the lights were turned on (corrected for deposition). The smaller active fraction when deposited on the wall can be explained by a physical surface reduction during the adhesion process of the droplets (possibly coagulating to larger droplets on the hydrophobic surface) and by an inhomogeneous irradiation of the chamber walls (especially the large fraction of wall surface perpendicular to the solar simulator), but also by a drying effect due to the heating of the Teflon walls during irradiation. Fig. 2 demonstrates the contribution of active, deposited surface on the wall to the total active surface area during the experiment with Fe^{III}-doped, pH-adjusted (pH 2.1–2.3) artificial seawater (Cl⁻/Fe^{III} = 101). The figure additionally includes dQ_{abs}/dt and Q_{abs} , which are discussed in the *Effect of pH and Fe^{III} speciation chemistry* section.

Iron(III)-catalysed Cl atom production

Significant Cl activation was detected for every sample with Cl⁻/Fe^{III} < 101 (Table 2), whereas Cl production was close to the detection limit during the blank experiments including Fe^{III}-free NaCl and artificial sea-salt aerosol in zero air. The effect of the constituents of the Fe^{III}-containing artificial seawater mixture was investigated by comparing the Cl release with a pure NaCl + FeCl₃ mixture. Both samples were prepared with a molar ratio of Cl⁻/Fe^{III} = 13. Both experiments were conducted in the same manner and under the same conditions (21 ± 1 °C and 72 ± 2 % RH). After 45 min of aerosol injection and a 15-min waiting period, the light was turned on. The aerosol size

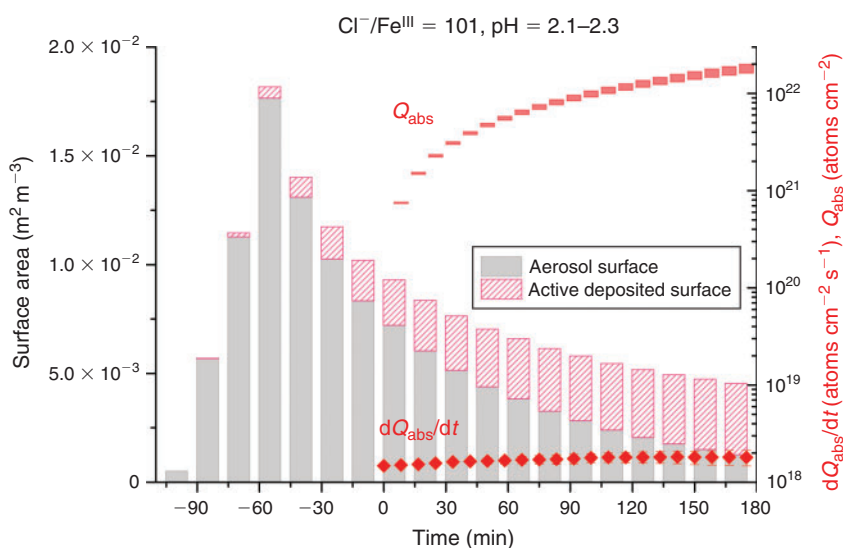


Fig. 2. Time profile of the sum of the total measured aerosol surface area and the active deposited surface during the experiment with Fe^{III}-doped, pH-adjusted (pH = 2.1–2.3) artificial seawater (Cl⁻/Fe^{III} = 101) and the corresponding absolute gaseous mean Cl production rate (dQ_{abs}/dt) (atoms cm⁻² s⁻¹) and time-integrated total Cl production Q_{abs} (atoms cm⁻²) of active aerosol surface. The light was switched on at 0 min.

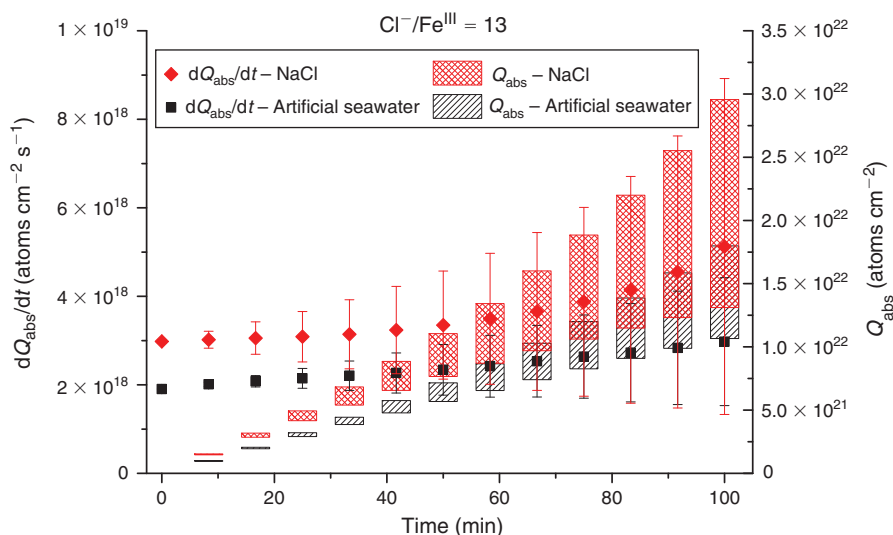


Fig. 3. Absolute gaseous mean Cl production rate (dQ_{aps}/dt) ($\text{atoms cm}^{-2} \text{s}^{-1}$) and time-integrated total minimum and maximum Cl production Q_{aps} (atoms cm^{-2}) of aerosol surface during the experiments with Fe^{III} -doped artificial seawater and NaCl with $\text{Cl}^-/\text{Fe}^{\text{III}} = 13$. The error bars for dQ_{aps}/dt include the minimum and maximum production rates and the respective statistical uncertainty. The light was switched on at 0 min.

distributions (Fig. 1) showed small differences, with a lower diameter for the most abundant particles but only a slightly lower surface-to-volume ratio for the artificial sea salt/ Fe^{III} mixture ($1.29 \times 10^7 \text{ m}^{-1}$) compared with the NaCl/ Fe^{III} mixture ($1.31 \times 10^7 \text{ m}^{-1}$) caused by the similar hydration behaviour at the given RH (Köhler theory).^[45] The Cl production rates and corresponding total production are shown in Fig. 3. Slightly higher Cl production of the pure NaCl/ Fe^{III} mixture was observed, which was probably caused by the speciation chemistry (as photolabile Fe^{III} -Cl complexes can form more easily in the absence of competing ions such as SO_4^{2-}).^[46] Considering the diluted stock solutions, the pH was between 1.9 and 2.2 for both experiments. The buffer effect of the added bicarbonate (0.2 g L^{-1}) in the artificial seawater is very low, considering the high amount of FeCl_3 added (13 g L^{-1}). Although the radical clock method is also able to quantify Br and OH, the depletion of HCs was dominated by Cl with its much higher reaction rate constants (Table S2, Supplementary material), which prevents significant interpretation of Br and OH (in most cases), which were close to the detection limit (Br $\sim 10^9 \text{ molecules cm}^{-3}$; OH $\sim 10^6 \text{ molecules cm}^{-3}$).

In order to determine the dependence of the chlorine activation on the $\text{Cl}^-/\text{Fe}^{\text{III}}$ ratio in the aerosol, a series of experiments with a $\text{Cl}^-/\text{Fe}^{\text{III}}$ ratio of (i) 13, (ii) 53, (iii) 101, (iv) 955 and (v) a blank without iron addition was conducted. Whereas no significant Cl concentration was detected for run (iv) and (v), (iii) resulted in a total Cl production of $(0.9\text{--}1.0) \times 10^{21} \text{ atoms cm}^{-2}$, run (ii) of $(2.3\text{--}2.6) \times 10^{21} \text{ atoms cm}^{-2}$, and run (i) of $(1.1\text{--}1.8) \times 10^{22} \text{ atoms cm}^{-2}$ in the first 100 min (Fig. 4). This demonstrates a continuous increase in produced Cl with increasing fraction of Fe^{III} in the salt. A 1.9-times higher fraction of Fe^{III} results in a 2–3-times higher Cl production (comparing (iii) and (ii)), and 4.1 times more Fe^{III} results in 5–7-times higher Cl production (comparing (ii) and (i)). The higher amount of added FeCl_3 cannot only explain the disproportionately higher Cl activation. In fact, the shift in pH from adding 10 times more FeCl_3 (pH 4 \rightarrow 2) is in addition responsible for a higher fraction of photolabile Fe^{III} -Cl complexes (discussed in the *Effect of*

pH and Fe^{III} speciation chemistry section). A slight decrease was observed for (iii), indicating exhaustion of the Cl source, whereas samples (i) and (ii) resulted in a more stable Cl production rate.

Effects of NO_2 , O_3 and SO_2

Experiments on the typical tropospheric traces and pollutants NO_2 , O_3 and SO_2 were performed by adding 20 ppb of NO_2 , 630 ppb of O_3 , and 20 and 200 ppb of SO_2 . These levels were chosen with the aim to better observe their effects and to obtain aerosol to pollutant ratios approximately comparable with natural conditions (discussed in the *Environmental significance* section). Figs 5 and 6 show the time profiles of the trace gases (corrected for dilution) combined with the results on Cl_{qs} , dQ_{aps}/dt and Q_{aps} obtained by the radical clock for the experiments with Fe^{III} -doped artificial seawater ($\text{Cl}^-/\text{Fe}^{\text{III}} = 13$) and addition of NO_2 and O_3 respectively. After the aerosol injection, the addition of NO_2 and a waiting period of 55 min (12 min in case of the O_3 experiment), the solar simulator was turned on (indicated by 0 min in the figures). For both experiments, significantly elevated Cl production was observed compared with the experiments in zero air. The higher Cl source is related to the additional activation mechanisms in the presence of O_3 and NO_x ,^[13] which are discussed in the following text. Fast formation of O_3 was observed in the NO_x experiment when the light was turned on, caused by the well-known photochemical cycle of NO, NO_2 and O_3 (photolysis rate coefficients: $J_{\text{NO}_2} = 6.7 \times 10^{-3} \text{ s}^{-1}$, $J_{\text{O}_3} = 2 \times 10^{-4} \text{ s}^{-1}$) on the one hand and the re-oxidation of NO to NO_2 and OH by HO_2 (formed by the depletion of the injected HCs) on the other hand. Therefore, the O_3 concentration exceeded the NO_x concentration in the course of the experiment, and the O_3 formation stopped when NO was depleted. Because O_3 is not present during the dark period, only negligible amounts of dark-phase nitrogen oxides like dinitrogen pentoxide (N_2O_5) could be present at the beginning of the irradiation and potentially explain the additional Cl source by the proposed heterogeneous activation mechanisms.^[12,13,32,47] During irradiation, the presence of O atoms and O_3 formation can cause the formation of NO_3

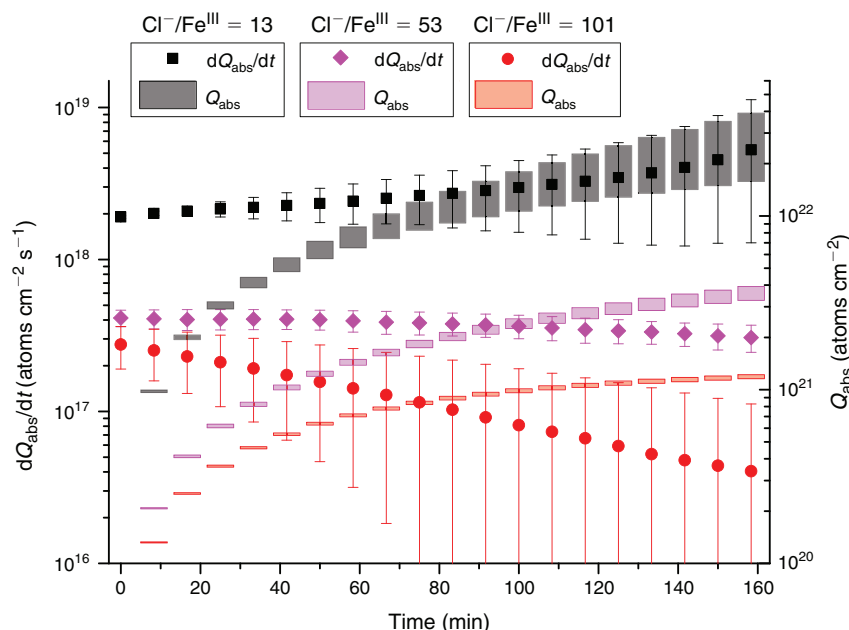


Fig. 4. Absolute gaseous mean Cl production rate (dQ_{abs}/dt) ($\text{atoms cm}^{-2} \text{s}^{-1}$) and time-integrated total minimum and maximum Cl production Q_{abs} (atoms cm^{-2}) of aerosol surface during the experiments with Fe^{III}-doped artificial seawater at various Fe^{III} concentrations: $\text{Cl}^-/\text{Fe}^{\text{III}} = 13$ (black), 53 (magenta), 101 (red). The light was switched on at 0 min.

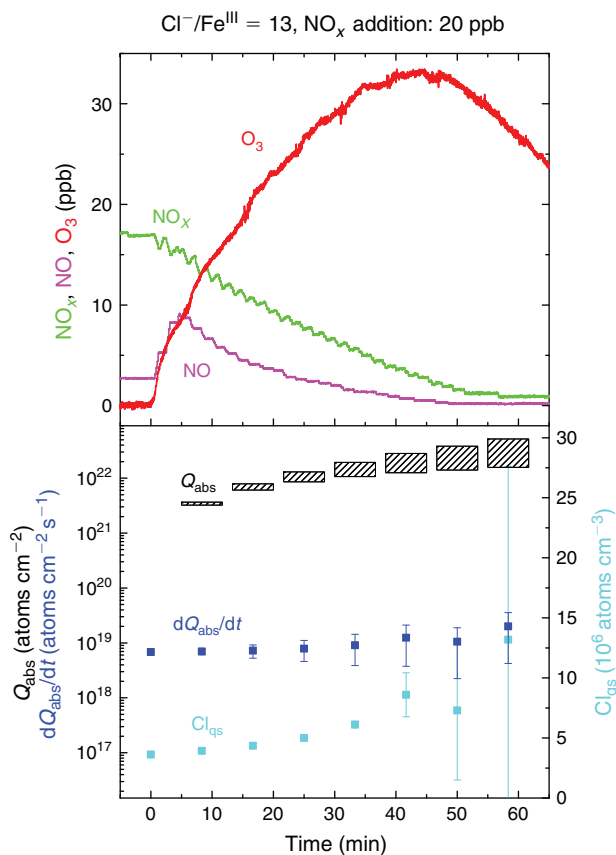
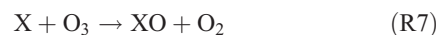


Fig. 5. Time profiles of NO_x , NO and O_3 (upper box) and of the quasi-stationary Cl concentration (Cl_{qs}), the absolute gaseous mean Cl production rate (dQ_{abs}/dt) ($\text{atoms cm}^{-2} \text{s}^{-1}$) and the time-integrated total minimum and maximum Cl production Q_{abs} (atoms cm^{-2}) of aerosol surface (lower box) during the experiment with Fe^{III}-doped artificial seawater ($\text{Cl}^-/\text{Fe}^{\text{III}} = 13$) and 20 ppb NO_x . The light was switched on at 0 min.

and thus N_2O_5 , although NO_3 is extremely short-lived under our conditions ($J_{\text{NO}_3} = 0.11 \text{ s}^{-1}$). At an NO_x concentration of 20 ppb, the proposed formation and photolysis of nitrosyl chloride (CINO) by NO_2 uptake of the sea-salt aerosol^[48–50] is too slow to contribute significantly to gaseous Cl production. For instance, Karlsson and Ljungström^[51] estimated a total CINO production of the order of $1.1 \times 10^7 \text{ atoms cm}^{-3}$ in a flow reactor at aerosol concentrations of $3 \times 10^5 \text{ cm}^{-3}$ (surface/volume = $2 \times 10^7 \text{ m}^{-1}$) when 50 ppb NO_2 was present. Owing to a photolysis rate of $J_{\text{CINO}} = 1.8 \times 10^{-3} \text{ s}^{-1}$ in our chamber, this would result in comparable Cl production, whereas the actual total production in our experiments is of the order of 10^{12} – $10^{13} \text{ atoms cm}^{-3}$ and thus exceeds the production caused by CINO formation by far, even if Karlsson and Ljungström^[51] assume a sea-salt surface three orders of magnitude lower. The negligible influence of NO_2 - or N_2O_5 -induced Cl activation was confirmed by a blank experiment (iron-free artificial sea salt with 20 ppb NO_2 addition), where the artificial sea-salt aerosol without Fe^{III} was irradiated in the presence of 20 ppb NO_x and the quasi-stationary Cl concentration remained below 10^4 molecules cm^{-3} combined with a slower NO_x depletion (Supplementary material, Fig. S2). Rather, the formation of XONO_2 ($\text{X} = \text{Cl}, \text{Br}$) by XO (R7, R8), or HNO_3 by OH (R9) and the subsequent uptake by the aerosol may explain the NO_x loss,^[12,31,52] which predominantly ends up as nitrate (with a possible back-reaction pathway to N_2O_5 or XNO_2 by HNO_3 at low pH).^[13]



The uptake of XONO_2 can result in additional X_2 or BrCl release, as e.g. summarised in the review by Rossi.^[13] The

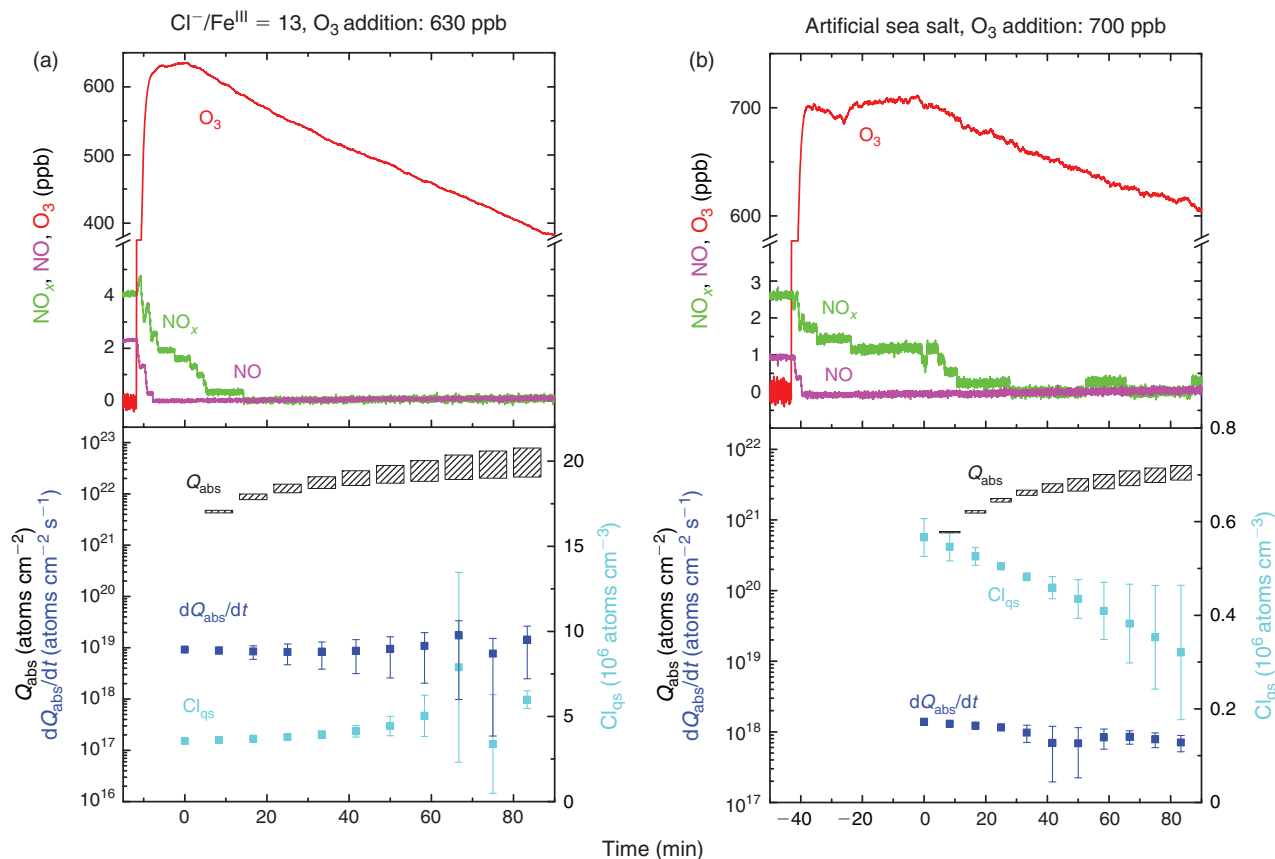


Fig. 6. Time profiles of NO_x, NO, and O₃ (upper box) and of the quasi-stationary Cl concentrations (Cl_{qs}), the absolute gaseous mean Cl production rate (dQ_{abs}/dt) ($\text{atoms cm}^{-2} \text{ s}^{-1}$) and of the time-integrated total minimum and maximum Cl production Q_{abs} (atoms cm^{-2}) of aerosol surface (lower box) during the experiment with (a) Fe^{III}-doped artificial seawater ($\text{Cl}^-/\text{Fe}^{\text{III}} = 13$) and 630 ppb O₃; and (b) a corresponding blank experiment with Fe^{III}-free artificial seawater and 700 ppb O₃. The light was switched on at 0 min.

uptake of HNO₃ leads to an acidification of the aerosol and contributes to the reoxidation of Fe^{II} to Fe^{III} through photolysis and OH[•] formation in the aqueous phase^[20] and thus is potentially responsible for the enhanced gaseous Cl production, according to the mechanisms described in the Introduction. Additionally, the uptake of HNO₃ leads to acid displacement with a subsequent release of HCl,^[53,54] whose reaction with OH is supposed to be a main Cl-atom source in the marine troposphere.^[55] In general, a low pH facilitates the release of HCl and other gaseous Cl precursors.^[25,31,56,57] For example, Keene and Savoie^[56] determined a gaseous HCl mixing ratio in the range of 0.1 ppb, and Keene et al.^[25] modelled HCl outgassing of 1 ppb day⁻¹ for acidified sea salt (pH 3). Transferred to our conditions with typical OH concentrations of 10^6 – 10^7 molecules cm^{-3} and a much higher LWC, this leads to gaseous Cl production rates in the range of 10^9 – 10^{10} $\text{atoms cm}^{-3} \text{ h}^{-1}$ and thus potentially contributes less than 10% to the observed Cl production. This accounts also for the HCl formation caused by hydrogen abstraction during the consumption of the injected HC_i by Cl atoms. Furthermore, Zetzsch and Behnke^[58] investigated photochemical Cl production rates from 200 to 500 ppb O₃ and 300 ppb HCl in the presence of NaCl, Fe₂O₃ and SiO₂ aerosol. They concluded that the heterogeneous Cl⁻ activation exceeds the Cl source from the gas-phase reaction of OH and HCl by far.

Several effects were observed in the experiment where 630 ppb O₃ was added (Fig. 6). The total Cl production per hour is three to five times higher than the value obtained from the Fe^{III}-containing sample in zero air and is similar to the NO_x

experiment (Table 2). However, the reactivity of O₃ towards Cl ($\sim 180 \text{ s}^{-1}$) is comparable with the total reactivity of the injected HC_i ($\sim 200 \text{ s}^{-1}$) and not considered in the calculation of the total production Q , as it does not represent a final sink but rather initiates a reaction cycle by HO₂ and HOCl where finally Cl₂ is produced.^[59,60] In addition, Sadanaga et al.^[27] observed enhanced O₃ uptake rates in the presence of water-soluble Fe^{III} in synthetic sea salt without irradiation. During the short dark period, O₃ depletion was hardly detectable, whereas we observed an approximately four times lower O₃ lifetime for the experiment with added Fe^{III} ($\sim 10^4 \text{ s}$) compared with the pure artificial sea-salt sample ($\sim 4 \times 10^4$). In general, the O₃ destruction is related to autocatalytic halogen activation where Br especially plays a dominant role.^[34] This difference possibly explains the much higher Cl and Br production (Fig. 6a, b) at the same level of quasi-stationary OH concentrations ($\sim 10^7$ molecules cm^{-3}) for both experiments. Concerning Br production, the quasi-stationary Br concentration was again of the order of 10^9 atoms cm^{-3} (close to the detection limit) and resulted in Q_{abs} values of $(1\text{--}3) \times 10^{21}$ $\text{atoms cm}^{-2} \text{ h}^{-1}$ for the iron-free and $(3\text{--}8) \times 10^{21}$ $\text{atoms cm}^{-2} \text{ h}^{-1}$ for the iron-doped sea salt. Adding O₃ to the iron-free aerosol, the significant enhancement in Cl production ($\sim 3\text{--}4.5 \times 10^{21}$ $\text{atoms cm}^{-2} \text{ h}^{-1}$ from the iron-free sample in zero air to the iron-free sample with O₃ addition) is relatively low compared with the much stronger increase in Cl production when adding O₃ to the iron-containing sample ($1\text{--}4 \times 10^{22}$ $\text{atoms cm}^{-2} \text{ h}^{-1}$ from the iron-containing sample in zero air to the iron-containing sample with O₃ addition).

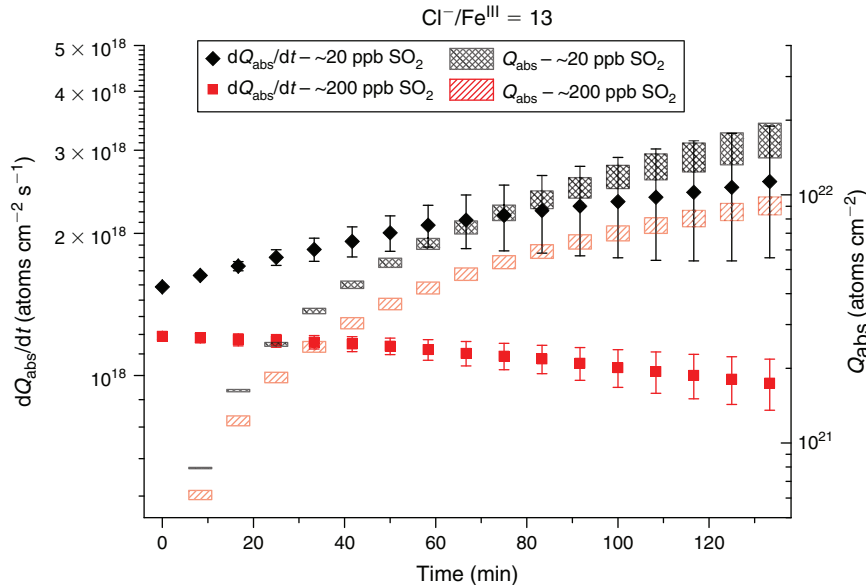
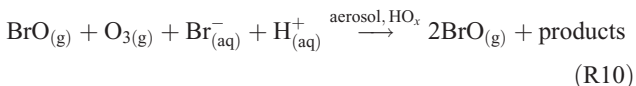


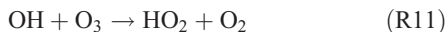
Fig. 7. Absolute gaseous mean Cl production rate (dQ_{abs}/dt) ($\text{atoms cm}^{-2} \text{s}^{-1}$) and time-integrated total minimum and maximum Cl production Q_{abs} (atoms cm^{-2}) of aerosol surface during experiments with Fe^{III}-doped artificial seawater ($\text{Cl}^-/\text{Fe}^{\text{III}} = 13$) and different SO₂ mixing ratios in the chamber (~ 20 ppb, red; ~ 200 ppb, black). The light was switched on at 0 min.

This indicates that we observed an O₃-induced Cl and Br production that increases with addition of Fe^{III} (or decreasing aerosol pH) and contributes markedly to the enhanced iron-induced activation. Several mechanisms come into consideration for the observed effects. At these O₃ levels, a main mechanism (which is responsible for the high Cl and Br production and fast O₃ depletion) is the so-called ‘Bromine explosion’^[61] with the net reaction:



and the associated formation of OClO and ClO.^[34] However, it does not sufficiently explain the increase in production rates from $\sim 2 \times 10^{18}$ to $\sim 10^{19}$ $\text{atoms cm}^{-2} \text{s}^{-1}$ with O₃ addition when Fe^{III} is involved (Figs 3 and 6a), because the pH (when < 5) is supposed to have no large effect on the mechanism,^[25,62] and the additional Cl production rate (when estimated from the iron-free experiment) is $\sim 10^{18}$ $\text{atoms cm}^{-2} \text{s}^{-1}$ (Fig. 6b).

A further approach is the enhanced formation of H₂O₂ in the gas phase (R11, R12):



which enters the aqueous phase rapidly and oxidises Fe^{II} back to Fe^{III}, and is able to form HOCl⁻ or HOBr⁻, which further dissociate and finally form Cl₂ or Br₂.^[63]

Knipping et al.^[64] even report a direct uptake of OH and subsequent Cl₂ release from NaCl aerosols. Furthermore, NO_x (3–5 ppb is present after aerosol injection) forms NO₃ and N₂O₅ by O₃ during the dark phase, indicated by the loss of NO_x when O₃ is injected (Fig. 6a, b), and thus leads to HNO₃ formation in the aqueous phase with similar consequences to those described above (R9). NO₃ is able to efficiently produce atomic X from solid and humidified salts.^[65,66] Moreover, the uptake of N₂O₅

activates Cl⁻ by releasing ClNO₂^[47,67] (or even Cl₂ in a multi-stage process by ClNO₂ at acidic pH)^[68] and Br⁻ by releasing Br₂ or BrNO₂,^[69,70] which is photolysed to atomic X ($J_{\text{ClNO}_2} = 0.2 \times 10^{-3} \text{s}^{-1}$, $J_{\text{BrNO}_2} = 3.7 \times 10^{-3} \text{s}^{-1}$, $J_{\text{Br}_2} = 17 \times 10^{-3} \text{s}^{-1}$). However, considering the low NO_x concentrations, the dark-phase activation mechanisms by NO₃ and N₂O₅ probably play an only minor role compared with autocatalytic light-induced activation. All given mechanisms favour the activation of bromide and could explain the high Br production rates in both O₃ experiments.

In contrast to the reinforcing effects of NO_x and O₃, the situation changes with SO₂. Two experiments were conducted with SO₂ concentrations of ~ 20 and ~ 200 ppb and a waiting period of 45 min before turning the solar simulator on. Similarly to the effect of sulfate in a salt pan,^[15] SO₂ inhibited Cl production, because slightly lower dQ_{abs}/dt and Q_{abs} were observed (Fig. 7). Several studies have already examined the role and the uptake of SO₂ in combination with Fe^{III} and Fe^{II} for seawater. For example, Hoppel et al.^[28] report an uptake of 0.21–1.2 mmol L⁻¹ of nebulised seawater, which is in a similar range to the sulfate concentration of 1 mmol L⁻¹ in the artificial seawater stock solution (which is nebulised in our case). However, we used a 29-times diluted stock solution to obtain size distributions with a maximum diameter of 400–450 nm. Additionally, the dissolution of SO₂ depends on further dissociation reactions in the aqueous phase that depend on pH, temperature and ion content.^[71] Therefore, the uptake rate of Hoppel et al. is only transferable with caution, but considering the less-concentrated stock solution, it should only be a small amount of SO₂ that dissolves in the aqueous phase of the aerosol, mainly in the form of bisulfite (HSO₃⁻) given the pH range (2–6) of our samples. Especially at a low pH, where a high portion of dissolved Fe³⁺ is available, the oxidation of sulfite to sulfate is catalysed by Fe³⁺.^[29] Moreover, a significant oxidation path is the reaction of sulfite with HOCl and HOBr, both of which can intervene in the autocatalytic halogen release.^[72,73] Although sulfate can strongly inhibit halogen activation, the effect of the

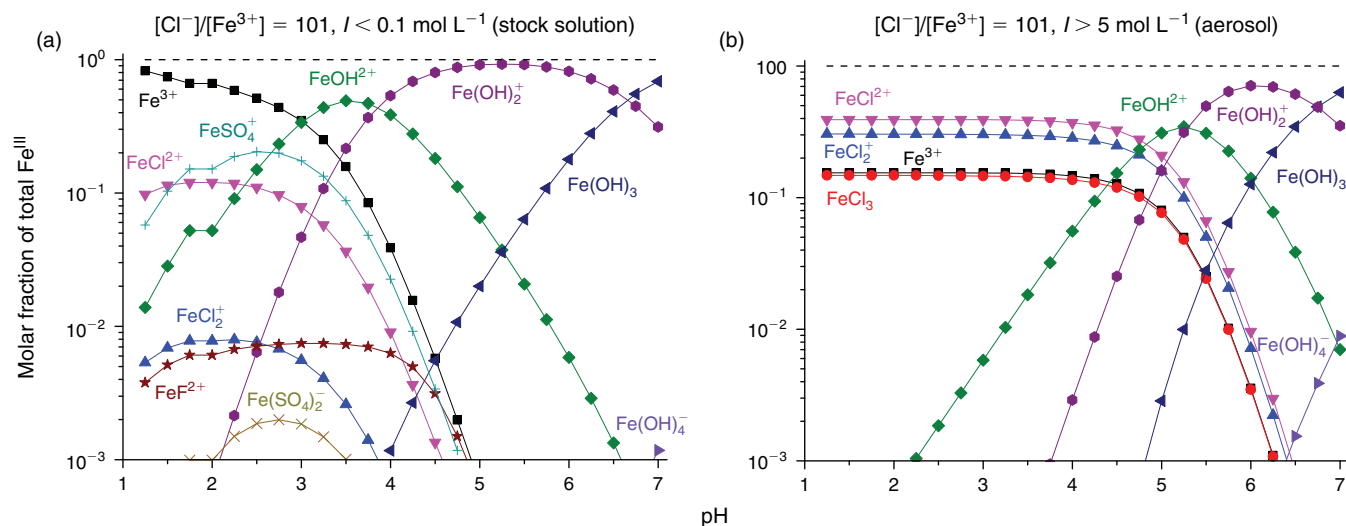


Fig. 8. Molar fraction of the formed Fe^{III} species relative to the total Fe^{III} content in Fe^{III}-doped artificial seawater (Cl⁻/Fe^{III} = 101) as a function of pH (according to the PHREEQC model) of the low-concentration diluted stock solution before nebulising (a); and of the final, highly concentrated aqueous phase of the aerosol (b). The dashed line indicates a molar fraction of 1 (100%).

freshly dissolved and oxidised SO₂ is probably very low with respect to the amount of sulfur that is already present in the artificial sea salt (*Sample preparation and chemicals used* section). A further influence of SO₂ is observed, concerning the quasi-stationary OH concentrations that are close to the detection limit of 10⁶ molecules cm⁻³ for both experiments, due to the oxidation of SO₂ in the gas phase (SO₂ + OH → HOSO₂; k = 1.3 × 10⁻¹² cm³ molecules⁻¹ s⁻¹),^[74] which competes with Cl production by HCl + OH (k = 7.8 × 10⁻¹³ cm³ molecules⁻¹ s⁻¹).^[75] Therefore, slightly lower Cl production is observed for the SO₂ experiments. In the extreme case of 200 ppb, Cl production decreases to ~70% of that from the SO₂-free experiment.

Effect of pH and Fe^{III} speciation chemistry

To estimate the effect of the aerosol pH on Cl production, the pH of the diluted stock solution (Cl⁻/Fe^{III} = 101) was adjusted to pH 2.1–2.3 by gently adding 32% HCl. The results demonstrate the immense effect of the pH (Fig. 2). The higher absolute production rate during the low-pH experiment led to eight times higher total Cl production per hour compared with the unadjusted sample (pH 3.9–4.2, Fig. 4; see also Table 2). There are multiple reasons for this effect. As evaluated in several studies for Fe^{III}-doped salts, the speciation chemistry of Fe^{III} strongly depends on the pH and ionic strength.^[15,24,76] Fig. 8a, b show the portions of the total Fe^{III} as Fe^{III} complexes as a function of the pH, calculated with an equilibrium model in PHREEQC.^[77] According to Wittmer et al., the model is based on the MINTEQ database,^[78] and the activity coefficients are corrected by the Pitzer ion interaction approach^[79] with the parameters listed in Tosca et al.^[80] The main equilibrium constants involving Fe^{III} are listed in the Supplementary material (Table S3). For some ions (e.g. F⁻), there are no Pitzer parameters available and the extended Debye–Hückel equation^[81,82] was applied to calculate the respective activity coefficients. To get an insight into the processes during nebulisation and evaporation, the speciation was calculated for the diluted stock solution (Fig. 8a), which the nebuliser was filled with, as well as for the final aerosol (Fig. 8b), assuming a saturation in Cl⁻ (6.1 mol L⁻¹) and unchanged molar ratios towards the other constituents. This

assumption is extremely simplified based on the complexity of a multicomponent salt system,^[45] and implies a similar hydration and solubility behaviour of NaCl and artificial sea salt but accounts for the fact that Na⁺ and Cl⁻ represent by far the main ions. For example, McCaffrey et al.^[83] measured similar Cl⁻ saturation concentrations in evaporating seawater whereas the concentration may change with increasing Fe^{III} content.

Whereas high fractions of Fe³⁺ ions and Fe^{III}-hydroxy complexes are present in the stock solution, the decisive photosensitive Fe^{III}-Cl complexes start to form as a considerable fraction at pH 1–4.5 with increasing ionic strength (solvent concentrations). The pH of 4.5 is a turning point for the aerosol speciation, where mainly Fe^{III}-hydroxy complexes are present. Because Fe^{III}-Cl complexes comprise a fraction of less than 5% in the stock solution at the given pH of 3.9–4.2 (and it takes some time until speciation equilibrium is reached during the transition from the low-concentration stock solution to the high-concentration liquid aerosol), the smaller amount of Fe^{III}-Cl complexes could explain the lower gaseous Cl production for the untreated sample. This situation changes when the pH is adjusted to 1.9–2.2 already in the diluted stock solution. At such low pH values, Fe^{III}-Cl complexes are formed much more easily. Furthermore, the solubility of Fe^{III} increases with decreasing pH, whereas more dissolved Fe^{III} becomes available on an absolute scale.^[46,84] Also, the formation of the highly soluble hypochlorous acid (HOCl; Henry's law constant at 298 K: 2.6–9.3 × 10² M atm⁻¹)^[85] predominates at a pH between 4 and 7 over Cl₂, which is favoured at a pH lower than 4 and is much more easily released into the gas phase (Henry's law constant: 6.2–9.1 × 10⁻² M atm⁻¹).^[85] Similar observations were also made by Lim et al.,^[24] who ascribed the decreasing Cl₂ source with decreasing pH to the speciation chemistry and solubility of the various chlorine species.

SEM-EDX results

Aerosol particles originating from the pure artificial sea water are mainly composed of NaCl, CaSO₄, MgCl₂ and KCl (Fig. 9a). Whereas NaCl and CaSO₄ particles remain as single crystals, KCl and MgCl₂ exhibit some phase-mixing and a more amorphous structure. In the case of the FeCl₃-containing artificial

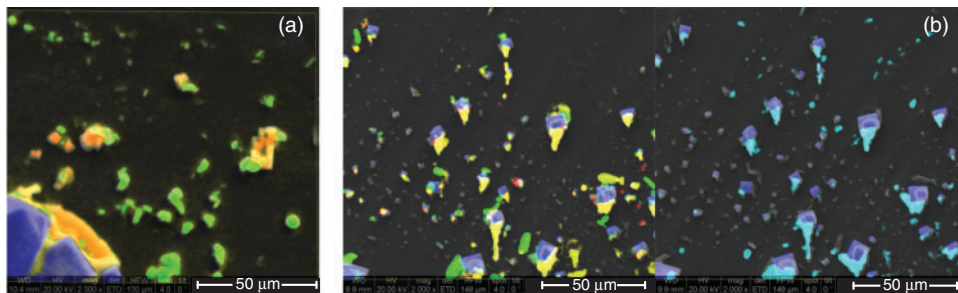


Fig. 9. Scanning electron microscope–energy dispersive X-ray (SEM-EDX) images of the aerosol particles of the pure sea-water (a), and FeCl₃-containing sea-water (b) with NaCl (blue), CaSO₄ (green), MgCl₂ (yellow), KCl (red) and FeCl₃ (turquoise).

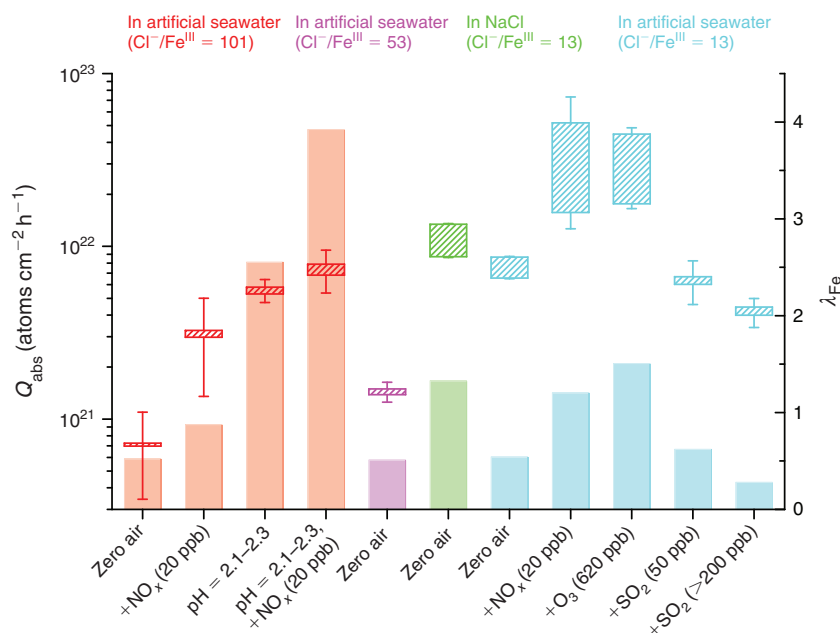


Fig. 10. Overview of the minimum and maximum absolute Cl production Q_{abs} (atoms $\text{cm}^{-2} \text{h}^{-1}$) over the first hour and the corresponding fraction of active Fe^{III} (λ_{Fe}) for each experiment with Fe^{III}-containing samples and various air contaminants (NO_x, O₃, SO₂).

seawater, single NaCl and CaSO₄ crystals are also visible. Additionally, FeCl₃ is visible in the KCl–MgCl₂ phase (Fig. 9b). FeCl₃ appears to cover nearly all other particles like NaCl and CaSO₄, thus indicating that all aerosol particles originating from the FeCl₃-enriched artificial seawater are covered by an active Fe^{III} chloride–salt layer.

Fraction of active iron

Multiplying the initial LWC_0 ($\text{dm}^3 \text{cm}^{-3}$) with the assumed saturation concentration of Cl[−] (6.1 mol L^{-1}) in the aerosols produced and with Avogadro’s constant ($N_A = 6 \times 10^{23} \text{ mol}^{-1}$) and dividing the molar Cl[−]/Fe^{III} ratio ($R_{\text{Cl/Fe}}$) in the stock solution yields the concentration of Fe^{III} in the chamber. The ratio of the minimum concentration of Cl atoms produced in the first hour of the experiments (Q_{min}) provides an estimation of the minimum fraction of active iron λ_{Fe} involved in Cl production:

$$\lambda_{\text{Fe}} = \frac{Q_{\text{min}} \times R_{\text{Cl/Fe}}}{LWC_0 \times 6.1 \times N_A} \quad (4)$$

assuming that each Fe^{III} produces 1/2Cl₂ by excluding recycling effects and secondary activation mechanisms. Owing to these major assumptions and unknown uncertainties ($R_{\text{Cl/Fe}}$ in the aerosol can differ from the bulk, or the concentration of Cl[−] can vary depending on the composition and thus deliquescence of the aerosol), λ_{Fe} represents a rather qualitative value for relative comparisons between the experiments. The contribution of the tare volume of the ions to the measured LWC is $0.11 \text{ m}^3 \text{m}^{-3}$ (considered in the calculation), whereas the influence of Fe³⁺ ions is negligible. Fig. 10 shows the results for all Fe^{III}-containing samples investigated, combined with the measured total minimum and maximum Cl production Q_{abs} during the first hour. Additionally, the corresponding initial minimum production rates are displayed in the Supplementary material (Fig. S3). Again, the increase in Q_{abs} for the artificial seawater samples with increasing Fe^{III} concentration (Cl[−]/Fe^{III} = 13, 53, 101) is highlighted, although, λ_{Fe} is comparable, which indicates that similar Cl activation mechanisms are going on. This is also the case for the pure NaCl + Fe^{III} sample where Q_{abs} and λ_{Fe} are higher, caused by the absence of

competing ligands for Fe^{III} and thus a higher fraction of photolabile Fe^{III}-Cl complexes.

The presence of 20 ppb NO_x in the gas phase led to a considerable increase by a factor of 3–7 for Q_{abs} from the Cl⁻/Fe^{III} = 101 and the Cl⁻/Fe^{III} = 13 samples. The parallel increase of λ_{Fe} (even more than 100%) is an artefact that actually represents the additional Cl activation mechanisms induced by NO_x,^[13] as discussed in the *Effects of NO₂, O₃ and SO₂* section. The same applies for the experiment with 630 ppb O₃. Decreasing the pH enhanced the activity of Fe^{III}, and more than 100% of Fe^{III} seemed to be involved, which either is a consequence of recycling effects (re-oxidation of Fe^{II} that was formed by photolysis of Fe^{III} complexes), or is caused by the uncertainty of λ_{Fe} . For the low-pH sample as well as for the untreated samples (Cl⁻/Fe^{III} = 13 and 101), an increase in Q_{abs} and λ_{Fe} was observed with the addition of 20 ppb NO_x, which clearly demonstrates the NO_x-induced activation of chloride. The effect is not as pronounced at low aerosol pH.

SO₂ was able to slightly inhibit Cl production. In particular, high SO₂ mixing ratios decreased the Q_{abs} and thus the fraction of active iron. One can compare λ_{Fe} with the salt-pan measurements, where a proportion of 0.05–0.07% of active Fe^{III} was determined.^[15] Considering a salt pan containing 0.5 g FeCl₃·6H₂O and 99.5 g NaCl results in a total molar Fe^{III} content of 1.8×10^{-3} . This is quite high compared with the aerosol experiments with only $\sim 3 \times 10^{-6}$ mol Fe^{III} at an LWC of $\sim 2.7 \times 10^{-9}$ but total Cl sources comparable with the salt-pan experiments. These large differences prove the small active surface area of the salt pans compared with the homogeneously distributed and irradiated aerosol in the chamber.

Environmental significance

The ratio of the concentrations of added pollutants and the generated aerosol concentrations (2–6 mg m⁻³) are approximately in agreement with the conditions for sea-salt aerosol over the ocean. Although the smog chamber helps to understand the mechanisms, it is difficult to transfer the results to large-scale atmospheric processes because the aerosol surface-to-volume ratio in the smog chamber is some orders of magnitude higher than in the atmosphere.

We investigated a very simplified system with no organic contaminants in the salt and under hydrocarbon-free conditions. Note that Fe complexes with oxygen-containing organics (such as phenolic compounds) can significantly increase the solubility of iron in seawater.^[86] However, complexation can strongly inhibit iron-induced chlorine activation,^[15] until the phenolic constituents are oxidised by OH[•] and Cl[•] from the photo-Fenton mechanism to the less-inhibiting but solubility-promoting oxalate. The soluble fraction of iron over the ocean ranges from 0 to 95% as the bulk marine aerosol type reflects a mixing of multiple aerosol types, and solubility varies with the origin of the iron, aerosol size and composition.^[87–89] Moreover, the solubility increases owing to the photoreduction of Fe^{III}, which is responsible for an Fe^{II} fraction in the aerosol of up to 50% in remote marine areas.^[90] An additional crucial factor for the role of Fe^{III} photochemistry is the aerosol pH, which varies from 1–9, mainly depending on the origin and age of the aerosol and the corresponding altering processes.^[25,56]

Accounting for these effects in order to quantify iron-induced Cl production in the troposphere, a sophisticated large-scale model would be required. Based on a mean molar Cl⁻/Fe ratio of 100–200 in the marine aerosol (central Atlantic),^[91] on the

lower fraction of dissolved Fe^{III} in the aerosol that can form photolabile complexes, and on the 20–200-times larger aerosol surface area in the chamber compared with the Atlantic aerosol,^[92] the mean natural contribution of Fe^{III}-induced Cl activation cannot compete with alternative mechanisms on a global scale (also indicated by Cl below the detection limit in our experiment with Cl⁻/Fe^{III} = 997). However, it may become important on a local scale with a larger Fe^{III} burden exposed to saline media, e.g. ship plumes or other iron-containing combustion aerosols^[93] or where soil dust comes into contact with sea salt, but also in brine-containing soils^[94] or salt lakes such as the Dead Sea or Australian salt lakes.^[14]

Furthermore, iron-doped sea-salt aerosols have been proposed as a method for climate engineering, aiming to enhance CH₄ depletion with higher Cl levels in the marine boundary layer and to simultaneously fertilise the oceans.^[95] Based on our results, one may try to estimate the feasibility of such a project. For our conditions, increasing the mean molar Cl⁻/Fe^{III} ratio to, say, 50 by adding Fe^{III} would have significant effects on Cl production and thus reduce the lifetime of CH₄. Transferred to the global production rate of sea salt Cl⁻ of 1785 Tg year⁻¹,^[96] an annual contribution of 56 Tg year⁻¹ of pure Fe^{III} (that dissolves totally in the sea-salt aerosol) would be needed. In addition, the effect of enhanced Cl production has to be scaled down by the much lower typical aerosol surface in the marine boundary layer (~ 60 – $200 \mu\text{m}^2 \text{cm}^{-3}$ ^[91]) compared with our experiments ($\sim 10\,000$ – $30\,000 \mu\text{m}^2 \text{cm}^{-3}$). Thus, an increase of Cl surface production by a factor of 4 in the chamber (which is the case for Cl⁻/Fe^{III} = 51 compared with the blank) would result in an increase of $\sim 2.5\%$ transferred to the marine boundary layer, neglecting any effect of dissolved organics or gas-phase species. A mixture with Cl⁻/Fe^{III} = 13 would need 220 Tg year⁻¹ of Fe^{III} and result in ~ 17 – 19% increase in Cl production. Note that the increase of atomic Cl does not directly correlate with a reduction of the CH₄ lifetime owing to the flat vertical profile of CH₄ (almost evenly distributed over the total troposphere)^[91] compared with the Cl-producing sea salt (confined to <1 km above the oceans, the marine sea-salt layer)^[91] and thus more inefficient depletion, apart from technical challenges and other potential implications for the ecosystem.

see below!

Conclusions

In the present work, we confirmed and quantified Cl formation processes induced by the photochemistry of Fe^{III} dissolved in the liquid aerosol phase. We found that depending on the Fe^{III} loading in the artificial sea-salt aerosol, an enormous amount of chlorine can be activated. The initial production rates varied from $\sim 1.9 \times 10^{18}$ atoms cm⁻² s⁻¹ (Cl⁻/Fe^{III} = 13) to $\sim 2.8 \times 10^{17}$ atoms cm⁻² s⁻¹ (Cl⁻/Fe^{III} = 101), whereas no significantly enhanced Cl production was detected for Cl⁻/Fe^{III} = 955 compared with the Fe^{III}-free salt. The differences can mainly be explained by the amount of Fe^{III} and the corresponding speciation of Fe^{III} complexes that depend on the pH.

The presence of 20 ppb NO_x or 630 ppb O₃ considerably increased the initial Cl production rate to $\sim 7 \times 10^{18}$ atoms cm⁻² s⁻¹ (Cl⁻/Fe^{III} = 13) and $\sim 9 \times 10^{18}$ atoms cm⁻² s⁻¹ (Cl⁻/Fe^{III} = 13) respectively (as compared with the blank value of 2×10^{18} atoms cm⁻² s⁻¹), owing to the well-known halogen activation processes and potential pH effects. Gas-phase SO₂ instead slightly inhibited Cl production to ~ 1.7 and $\sim 1.1 \times 10^{18}$ atoms cm⁻² s⁻¹, by adding ~ 20 ppb and >200 ppb SO₂ respectively. The strong effect of the aerosol pH on Fe^{III}

speciation and subsequent Cl formation was demonstrated by comparing two samples with an equal Cl⁻/Fe^{III} ratio of 101 but a pH adjusted to 2.1–2.3 and 3.9–4.2. Here, the production rate increased by almost an order of magnitude for the more acidic pH. An approach to calculate the active fraction of Fe^{III} involved in Cl production confirms a higher λ_{Fe} with lower pH, highlights recycling effects and identifies additional activation mechanisms where NO_x and O₃ are involved. In natural environments, these processes may occur in natural salty media at high dissolved Fe^{III} concentrations and locally contribute to photochemical Cl formation.

Supplementary material

The supplementary material (available on the journal's website at http://www.publish.csiro.au/?act=view_file&file_id=EN14279_AC.pdf) includes more details on the artificial seawater composition (Table S1), the rate constants of the applied HCs towards the radicals (Table S2), the main equilibrium constants for important Fe^{III} complexes, the contour plots of selected experiments (Fig. S1), the NO_x, NO, and O₃ time profiles for the Fe^{III}-free experiment with 20 ppb NO₂ addition (Fig. S2) and an overview of the initial minimum absolute Cl production rate (Fig. S3).

Acknowledgements

We thank Franz D. Oeste, gM-Ingenieurbüro Kirchhain, Germany, for advice, Agnes Bednorz and Andrej Einhorn for technical support and Elisabeth Eitenberger and Gernot Friedbacher (Vienna University of Technology) for operating the electron microscope. This work was supported by the Deutsche Forschungsgemeinschaft (DFG) within research unit 763 (HALOPROC) and by Ries Consulting GmbH&Co Betriebs KG, Hosenfeld.

References

- [1] I. Y. Fung, S. K. Meyn, I. Tegen, S. C. Doney, J. G. John, J. K. B. Bishop, Iron supply and demand in the upper ocean. *Global Biogeochem. Cycles* **2000**, *14*, 281. doi:10.1029/1999GB900059
- [2] M. S. Johnson, N. Meskhidze, Atmospheric dissolved iron deposition to the global oceans: effects of oxalate-promoted Fe dissolution, photochemical redox cycling, and dust mineralogy. *Geosci. Model Dev.* **2013**, *6*, 1137. doi:10.5194/GMD-6-1137-2013
- [3] A. Martínez-García, D. M. Sigman, H. Ren, R. F. Anderson, M. Straub, D. A. Hodell, S. L. Jaccard, T. I. Eglinton, G. H. Haug, Iron fertilization of the subantarctic ocean during the last Ice Age. *Science* **2014**, *343*, 1347. doi:10.1126/SCIENCE.1246848
- [4] A. Martínez-García, A. Rosell-Melé, S. L. Jaccard, W. Geibert, D. M. Sigman, G. H. Haug, Southern Ocean dust–climate coupling over the past four million years. *Nature* **2011**, *476*, 312. doi:10.1038/NATURE10310
- [5] J. H. Martin, S. E. Fitzwater, R. M. Gordon, Iron deficiency limits phytoplankton growth in Antarctic waters. *Global Biogeochem. Cycles* **1990**, *4*, 5. doi:10.1029/GB0041001P00005
- [6] S. Blain, B. Quéguiner, L. Armand, S. Belviso, B. Bombled, L. Bopp, A. Bowie, C. Brunet, C. Brussaard, F. Carlotti, U. Christaki, A. Corbière, I. Durand, F. Ebersbach, J.-L. Fuda, N. Garcia, L. Gerringa, B. Griffiths, C. Guigue, C. Guillemer, S. Jacquet, C. Jeandel, P. Laan, D. Lefèvre, C. Lo Monaco, A. Malits, J. Mosseri, I. Obernosterer, Y.-H. Park, M. Picheral, P. Pondaven, T. Remyenyi, V. Sandroni, G. Sarthou, N. Savoye, L. Scouarnec, M. Souhaut, D. Thuiller, K. Timmermans, T. Trull, J. Uitz, P. van Beek, M. Veldhuis, D. Vincent, E. Viollier, L. Vong, T. Wagener, Effect of natural iron fertilization on carbon sequestration in the Southern Ocean. *Nature* **2007**, *446*, 1070. doi:10.1038/NATURE05700
- [7] R. T. Pollard, I. Salter, R. J. Sanders, M. I. Lucas, C. M. Moore, R. A. Mills, P. J. Statham, J. T. Allen, A. R. Baker, D. C. E. Bakker, M. A. Charette, S. Fielding, G. R. Fones, M. French, A. E. Hickman, R. J. Holland, J. A. Hughes, T. D. Jickells, R. S. Lampitt, P. J. Morris, F. H. Nedelec, M. Nielsdottir, H. Planquette, E. E. Popova, A. J. Poulton, J. F. Read, S. Seeyave, T. Smith, M. Stinchcombe, S. Taylor, S. Thomalla, H. J. Venables, R. Williamson, M. V. Zubkov, Southern Ocean deep-water carbon export enhanced by natural iron fertilization. *Nature* **2009**, *457*, 577. doi:10.1038/NATURE07716
- [8] R. von Glasow, P. J. Crutzen, Tropospheric halogen chemistry, in *Treatise on Geochemistry* (Eds H. D. Holland, K. K. Turekian) **2003**, Vol. 4, pp 1–67 (Elsevier-Pergamon: Oxford, UK).
- [9] U. Platt, G. Hönninger, The role of halogen species in the troposphere. *Chemosphere* **2003**, *52*, 325. doi:10.1016/S0045-6535(03)00216-9
- [10] J. Ofner, N. Balzer, J. Buxmann, H. Grothe, P. Schmitt-Kopplin, U. Platt, C. Zetzsch, Halogenation processes of secondary organic aerosol and implications on halogen release mechanisms. *Atmos. Chem. Phys.* **2012**, *12*, 5787. doi:10.5194/ACP-12-5787-2012
- [11] R. von Glasow, Atmospheric chemistry: wider role for airborne chlorine. *Nature* **2010**, *464*, 168. doi:10.1038/464168A
- [12] B. J. Finlayson-Pitts, The tropospheric chemistry of sea salt: a molecular-level view of the chemistry of NaCl and NaBr. *Chem. Rev.* **2003**, *103*, 4801. doi:10.1021/CR020653T
- [13] M. J. Rossi, Heterogeneous reactions on salts. *Chem. Rev.* **2003**, *103*, 4823. doi:10.1021/CR020507N
- [14] T. Krause, C. Tubbesing, K. Benzing, H. F. Schöler, Model reactions and natural occurrence of furans from hypersaline environments. *Biogeosciences* **2014**, *11*, 2871. doi:10.5194/BG-11-2871-2014
- [15] J. Wittmer, S. Bleicher, C. Zetzsch, Iron(III)-induced activation of chloride and bromide from modeled salt pans. *J. Phys. Chem. A* **2015**, *119*, 4373. [Published online early 22 September 2014]. doi:10.1021/JP508006S
- [16] H. Fu, D. M. Cwiertny, G. R. Carmichael, M. M. Scherer, V. H. Grassian, Photoreductive dissolution of Fe-containing mineral dust particles in acidic media. *J. Geophys. Res.* **2010**, *115*, D11304. doi:10.1029/2009JD012702
- [17] X. Zhu, J. M. Prospero, D. L. Savoie, F. J. Millero, R. G. Zika, E. S. Saltzman, Photoreduction of iron(III) in marine mineral aerosol solutions. *J. Geophys. Res.* **1993**, *98*, 9039. doi:10.1029/93JD00202
- [18] W. L. Miller, D. King, J. Lin, D. R. Kester, Photochemical redox cycling of iron in coastal seawater. *Mar. Chem.* **1995**, *50*, 63. doi:10.1016/0304-4203(95)00027-0
- [19] R. L. Siefert, S. O. Pehkonen, Y. Erel, M. R. Hoffmann, Iron photochemistry of aqueous suspensions of ambient aerosol with added organic acids. *Geochim. Cosmochim. Acta* **1994**, *58*, 3271. doi:10.1016/0016-7037(94)90055-8
- [20] D. Vione, V. Maurino, C. Minero, E. Pelizzetti, M. A. Harrison, R.-I. Olariu, C. Arsene, Photochemical reactions in the tropospheric aqueous phase and on particulate matter. *Chem. Soc. Rev.* **2006**, *35*, 441.
- [21] V. A. Nadtochenko, J. Kiwi, Photolysis of FeOH²⁺ and FeCl²⁺ in aqueous solution. Photodissociation kinetics and quantum yields. *Inorg. Chem.* **1998**, *37*, 5233. doi:10.1021/IC9804723
- [22] A. Machulek, J. E. Moraes, L. T. Okano, C. A. Silvério, F. H. Quina, Photolysis of ferric ions in the presence of sulfate or chloride ions: implications for the photo-Fenton process. *Photochem. Photobiol. Sci.* **2009**, *8*, 985. doi:10.1039/B900553F
- [23] D. Whitney King, R. A. Aldrich, S. E. Charnecki, Photochemical redox cycling of iron in NaCl solutions. *Mar. Chem.* **1993**, *44*, 105. doi:10.1016/0304-4203(93)90196-U
- [24] M. Lim, K. Chiang, R. Amal, Photochemical synthesis of chlorine gas from iron(III) and chloride solution. *J. Photoch. Photobio. A: Chemistry* **2006**, *183*, 126. doi:10.1016/J.PHOTOCHEM.2006.03.005
- [25] W. C. Keene, R. Sander, A. A. Pszenny, R. Vogt, P. J. Crutzen, J. N. Galloway, Aerosol pH in the marine boundary layer. *J. Aerosol Sci.* **1998**, *29*, 339. doi:10.1016/S0021-8502(97)10011-8
- [26] J. De Laat, T. G. Le, Kinetics and modeling of the Fe^{III}/H₂O₂ system in the presence of sulfate in acidic aqueous solutions. *Environ. Sci. Technol.* **2005**, *39*, 1811. doi:10.1021/ES0493648
- [27] Y. Sadanaga, J. Hirokawa, H. Akimoto, Formation of molecular chlorine in dark condition: heterogeneous reaction of ozone with sea salt in the presence of ferric ion. *Geophys. Res. Lett.* **2001**, *28*, 4433. doi:10.1029/2001GL013722

- [28] W. Hoppel, L. Pasternack, P. Caffrey, G. Frick, J. Fitzgerald, D. Hegg, S. Gao, J. Ambrusko, T. Albrecht, Sulfur dioxide uptake and oxidation in sea-salt aerosol. *J. Geophys. Res.* **2001**, *106*, 27 575. doi:10.1029/2000JD900843
- [29] M. Novič, I. Grgič, M. Poje, V. Hudnik, Iron-catalyzed oxidation of S^{IV} species by oxygen in aqueous solution: influence of pH on the redox cycling of iron. *Atmos. Environ.* **1996**, *30*, 4191. doi:10.1016/1352-2310(96)00137-9
- [30] J.-Z. Zhang, F. J. Millero, The rate of sulfite oxidation in seawater. *Geochim. Cosmochim. Acta* **1991**, *55*, 677. doi:10.1016/0016-7037(91)90333-Z
- [31] S. Bleicher, J. C. Buxmann, R. Sander, T. P. Riedel, J. A. Thornton, U. Platt, C. Zetzsch, The influence of nitrogen oxides on the activation of bromide and chloride in salt aerosol. *Atmos. Chem. Phys. Discuss.* **2014**, *14*, 10 135. doi:10.5194/ACPD-14-10135-2014
- [32] W. Behnke, C. Zetzsch, Heterogeneous photochemical formation of Cl atoms from NaCl aerosol, NO_x and ozone. *J. Aerosol Sci.* **1990**, *21*, S229. doi:10.1016/0021-8502(90)90226-N
- [33] M. Brigante, M. Minella, G. Mailhot, V. Maurino, C. Minero, D. Vione, Formation and reactivity of the dichloride radical in surface waters: a modelling approach. *Chemosphere* **2014**, *95*, 464. doi:10.1016/J.CHEMOSPHERE.2013.09.098
- [34] J. Buxmann, N. Balzer, S. Bleicher, U. Platt, C. Zetzsch, Observations of bromine explosions in smog chamber experiments above a model salt pan. *Int. J. Chem. Kinet.* **2012**, *44*, 312. doi:10.1002/KIN.20714
- [35] W. Behnke, W. Holländer, W. Koch, F. Nolting, C. Zetzsch, A smog chamber for studies of the photochemical degradation of chemicals in the presence of aerosols. *Atmos. Environ.* **1988**, *22*, 1113. doi:10.1016/0004-6981(88)90341-1
- [36] D. R. Kester, I. W. Duedall, D. N. Connors, R. M. Pytkowicz, Preparation of artificial seawater. *Limnol. Oceanogr.* **1967**, *12*, 176. doi:10.4319/LO.1967.12.1.0176
- [37] K. Zhang, E. Knipping, A. Wexler, P. Bhave, G. Tonnesen, Size distribution of sea-salt emissions as a function of relative humidity. *Atmos. Environ.* **2005**, *39*, 3373. doi:10.1016/J.ATMOSENV.2005.02.032
- [38] N. Balzer, *Kinetische Untersuchungen der Halogen-Aktivierung einer simulierten Salzpfanne in einer Smogkammer* **2012**, Ph.D. thesis, University of Bayreuth, Germany.
- [39] P. Supeno, P. Kruus, Sonochemical formation of nitrate and nitrite in water. *Ultrason. Sonochem.* **2000**, *7*, 109. doi:10.1016/S1350-4177(99)00043-7
- [40] T. B. Ryerson, E. J. Williams, F. C. Fehsenfeld, An efficient photolysis system for fast-response NO₂ measurements. *J. Geophys. Res.* **2000**, *105*, 26 447. doi:10.1029/2000JD900389
- [41] N. A. Kelly, Characterization of fluorocarbon-film bags as smog chambers. *Environ. Sci. Technol.* **1982**, *16*, 763. doi:10.1021/ES00105A007
- [42] C. Misra, M. Singh, S. Shen, C. Sioutas, P. M. Hall, Development and evaluation of a personal cascade impactor sampler (PCIS). *J. Aerosol Sci.* **2002**, *33*, 1027. doi:10.1016/S0021-8502(02)00055-1
- [43] H. Lohninger, J. Ofner, Multisensor hyperspectral imaging as a versatile tool for image-based chemical structure determination. *Spectrosc. Eur.* **2014**, *26*, 6.
- [44] Y. Marcus, Ionic radii in aqueous solutions. *Chem. Rev.* **1988**, *88*, 1475. doi:10.1021/CR00090A003
- [45] I. N. Tang, A. C. Tridico, K. H. Fung, Thermodynamic and optical properties of sea-salt aerosols. *J. Geophys. Res.* **1997**, *102*, 23 269. doi:10.1029/97JD01806
- [46] F. J. Millero, Solubility of Fe^{III} in seawater. *Earth Planet. Sci. Lett.* **1998**, *154*, 323. doi:10.1016/S0012-821X(97)00179-9
- [47] J. A. Thornton, J. P. Kercher, T. P. Riedel, N. L. Wagner, J. Cozic, J. S. Holloway, W. P. Dubé, G. M. Wolfe, P. K. Quinn, A. M. Middlebrook, B. Alexander, S. S. Brown, A large atomic chlorine source inferred from mid-continental reactive nitrogen chemistry. *Nature* **2010**, *464*, 271. doi:10.1038/NATURE08905
- [48] W. H. Schroeder, P. Urone, Formation of nitrosyl chloride from salt particles in air. *Environ. Sci. Technol.* **1974**, *8*, 756. doi:10.1021/ES60093A015
- [49] B. J. Finlayson-Pitts, Reaction of NO₂ with NaCl and atmospheric implications of NOCl formation. *Nature* **1983**, *306*, 676. doi:10.1038/306676A0
- [50] W. Behnke, H.-U. Krüger, V. Scheer, C. Zetzsch, Formation of ClNO₂ and HONO in the presence of NO₂, O₃ and wet NaCl aerosol. *J. Aerosol Sci.* **1992**, *23*, 933. doi:10.1016/0021-8502(92)90565-D
- [51] R. Karlsson, E. Ljungström, Nitrogen dioxide and sea salt particles – a laboratory study. *J. Aerosol Sci.* **1995**, *26*, 39. doi:10.1016/0021-8502(94)00098-J
- [52] A. Saiz-Lopez, R. von Glasow, Reactive halogen chemistry in the troposphere. *Chem. Soc. Rev.* **2012**, *41*, 6448. doi:10.1039/C2CS35208G
- [53] D. O. De Haan, B. J. Finlayson-Pitts, Knudsen cell studies of the reaction of gaseous nitric acid with synthetic sea salt at 298 K. *J. Phys. Chem. A* **1997**, *101*, 9993. doi:10.1021/JP972450S
- [54] T. D. Saul, M. P. Tolocka, M. V. Johnston, Reactive uptake of nitric acid onto sodium chloride aerosols across a wide range of relative humidities. *J. Phys. Chem. A* **2006**, *110*, 7614. doi:10.1021/JP060639A
- [55] W. Behnke, V. Scheer, C. Zetzsch, Production of a photolytic precursor of atomic Cl from aerosols and Cl⁻ in the presence of O₃, in *Naturally Produced Organohalogen* (Eds A. Grimvall, E. de Leer) **1995**, pp. 375–384 (Springer: Dordrecht, Netherlands).
- [56] W. C. Keene, D. L. Savoie, The pH of deliquesced sea-salt aerosol in polluted marine air. *Geophys. Res. Lett.* **1998**, *25*, 2181. doi:10.1029/98GL01591
- [57] P. Brimblecombe, S. L. Clegg, The solubility and behaviour of acid gases in the marine aerosol. *J. Atmos. Chem.* **1988**, *7*, 1. doi:10.1007/BF00048251
- [58] C. Zetzsch, W. Behnke, Heterogeneous reactions of chlorine compounds, in *The Tropospheric Chemistry of Ozone in the Polar Regions* (Eds H. Niki, K. H. Becker) **1993**, pp. 291–306 (Springer: New York).
- [59] S. Pechtl, R. von Glasow, Reactive chlorine in the marine boundary layer in the outflow of polluted continental air: a model study. *Geophys. Res. Lett.* **2007**, *34*, L11813. doi:10.1029/2007GL029761
- [60] C. B. Faxon, D. T. Allen, Chlorine chemistry in urban atmospheres: a review. *Environ. Chem.* **2013**, *10*, 221. doi:10.1071/EN13026
- [61] M. Hausmann, U. Platt, Spectroscopic measurement of bromine oxide and ozone in the high Arctic during Polar Sunrise Experiment 1992. *J. Geophys. Res.* **1994**, *99*, 25 399. doi:10.1029/94JD01314
- [62] S. Fickert, J. W. Adams, J. N. Crowley, Activation of Br₂ and BrCl via uptake of HOBr onto aqueous salt solutions. *J. Geophys. Res.* **1999**, *104*, 23 719. doi:10.1029/1999JD900359
- [63] K. W. Oum, Formation of molecular chlorine from the photolysis of ozone and aqueous sea-salt particles. *Science* **1998**, *279*, 74. doi:10.1126/SCIENCE.279.5347.74
- [64] E. M. Knipping, M. J. Lakin, K. L. Foster, P. Jungwirth, D. J. Tobias, R. B. Gerber, D. Dabdub, B. J. Finlayson-Pitts, Experiments and simulations of ion-enhanced interfacial chemistry on aqueous NaCl aerosols. *Science* **2000**, *288*, 301. doi:10.1126/SCIENCE.288.5464.301
- [65] S. Seisel, F. Caloz, F. F. Fenter, H. van den Bergh, M. J. Rossi, The heterogeneous reaction of NO₃ with NaCl and KBr: a non-photolytic source of halogen atoms. *Geophys. Res. Lett.* **1997**, *24*, 2757. doi:10.1029/97GL02857
- [66] Y. Rudich, R. K. Talukdar, A. R. Ravishankara, R. W. Fox, Reactive uptake of NO₃ on pure water and ionic solutions. *J. Geophys. Res.* **1996**, *101*, 21 023. doi:10.1029/96JD01844
- [67] W. Behnke, C. George, V. Scheer, C. Zetzsch, Production and decay of ClNO₂ from the reaction of gaseous N₂O₅ with NaCl solution: bulk and aerosol experiments. *J. Geophys. Res.* **1997**, *102*, 3795. doi:10.1029/96JD03057
- [68] J. M. Roberts, H. D. Osthoff, S. S. Brown, A. R. Ravishankara, N₂O₅ oxidizes chloride to Cl₂ in acidic atmospheric aerosol. *Science* **2008**, *321*, 1059. doi:10.1126/SCIENCE.1158777
- [69] F. F. Fenter, F. Caloz, M. J. Rossi, Heterogeneous kinetics of N₂O₅ uptake on salt, with a systematic study of the role of surface presentation (for N₂O₅ and HNO₃). *J. Phys. Chem.* **1996**, *100*, 1008. doi:10.1021/JP9503829

- [70] B. J. Finlayson-Pitts, F. E. Livingston, H. N. Berko, Synthesis and identification by infrared spectroscopy of gaseous nitryl bromide, BrNO₂. *J. Phys. Chem.* **1989**, *93*, 4397. doi:10.1021/J100348A005
- [71] M. E. Gebel, B. J. Finlayson-Pitts, J. A. Ganske, The uptake of SO₂ on synthetic sea salt and some of its components. *Geophys. Res. Lett.* **2000**, *27*, 887. doi:10.1029/1999GL011152
- [72] R. Vogt, P. J. Crutzen, R. Sander, A mechanism for halogen release from sea-salt aerosol in the remote marine boundary layer. *Nature* **1996**, *383*, 327. doi:10.1038/383327A0
- [73] R. C. Troy, D. W. Margerum, Non-metal redox kinetics: hypobromite and hypobromous acid reactions with iodide and with sulfite and the hydrolysis of bromosulfate. *Inorg. Chem.* **1991**, *30*, 3538. doi:10.1021/IC00018A028
- [74] R. Atkinson, D. L. Baulch, R. A. Cox, J. N. Crowley, R. F. Hampson, R. G. Hynes, M. E. Jenkin, M. J. Rossi, J. Troe, Evaluated kinetic and photochemical data for atmospheric chemistry: Volume I – Gas-phase reactions of O₃, HO₂, NO_x and SO_x species. *Atmos. Chem. Phys.* **2004**, *4*, 1461. doi:10.5194/ACP-4-1461-2004
- [75] R. Atkinson, D. L. Baulch, R. A. Cox, J. N. Crowley, R. F. Hampson, R. G. Hynes, M. E. Jenkin, M. J. Rossi, J. Troe, Evaluated kinetic and photochemical data for atmospheric chemistry: Volume III – Gas-phase reactions of inorganic halogens. *Atmos. Chem. Phys.* **2007**, *7*, 981. doi:10.5194/ACP-7-981-2007
- [76] V. Nadochenko, J. Kiwi, Primary photochemical reactions in the photo-Fenton system with ferric chloride. 1. A case study of xylydine oxidation as a model compound. *Environ. Sci. Technol.* **1998**, *32*, 3273. doi:10.1021/ES970962E
- [77] D. L. Parkhurst, C. A. Appelo, *User's Guide to PHREEQC (Version 2): a Computer Program for Speciation, Batch-Reaction, One-Dimensional Transport, and Inverse Geochemical Calculations. Water Resource Investigations Report 1999*, pp. 99–4259 (US Geological Survey: Denver, CO, USA).
- [78] J. D. Allison, D. S. Brown, K. J. Novo-Gradac, *MINTEQA2/PRODEFA2, A Geochemical Assessment Model for Environmental Systems: Version 3.0 User's Manual 1991* (Environmental Research Laboratory, Office of Research and Development, US Environmental Protection Agency: Athens, GA).
- [79] K. S. Pitzer, Thermodynamics of electrolytes. I. Theoretical basis and general equations. *J. Phys. Chem.* **1973**, *77*, 268. doi:10.1021/J100621A026
- [80] N. J. Tosca, S. M. McLennan, B. C. Clark, J. P. Grotzinger, J. A. Hurowitz, A. H. Knoll, C. Schröder, S. W. Squyres, Geochemical modeling of evaporation processes on Mars: insight from the sedimentary record at Meridiani Planum. *Earth Planet. Sci. Lett.* **2005**, *240*, 122. doi:10.1016/J.EPSL.2005.09.042
- [81] A. H. Truesdell, B. F. Jones, WATEQ, a computer program for calculating chemical equilibria of natural waters. *US Geol. Surv. J. Res.* **1974**, *2*, 233.
- [82] E. Hückel, Zur Theorie konzentrierter wässriger Lösungen starker Elektrolyte. *Phys. Z.* **1925**, *26*, 93.
- [83] M. A. McCaffrey, B. Lazar, H. D. Ho, The evaporation path of seawater and the coprecipitation of Br⁻ and K⁺ with halite. *J. Sediment. Petrol.* **1987**, *57*, 928.
- [84] X. Liu, F. J. Millero, The solubility of iron in seawater. *Mar. Chem.* **2002**, *77*, 43. doi:10.1016/S0304-4203(01)00074-3
- [85] R. Sander, *Compilation of Henry's Law Constants for Inorganic and Organic Species of Potential Importance in Environmental Chemistry. Ver. 3 1999*. Available at <http://www.henrys-law.org/henry-3.0.pdf> [Verified May 2013].
- [86] K. Kuma, J. Nishioka, K. Matsunaga, Controls on iron(III) hydroxide solubility in seawater: the influence of pH and natural organic chelators. *Limnol. Oceanogr.* **1996**, *41*, 396. doi:10.4319/LO.1996.41.3.0396
- [87] E. R. Sholkovitz, P. N. Sedwick, T. M. Church, A. R. Baker, C. F. Powell, Fractional solubility of aerosol iron: synthesis of a global-scale data set. *Geochim. Cosmochim. Acta* **2012**, *89*, 173. doi:10.1016/J.GCA.2012.04.022
- [88] A. R. Baker, T. D. Jickells, M. Witt, K. L. Linge, Trends in the solubility of iron, aluminium, manganese and phosphorus in aerosol collected over the Atlantic Ocean. *Mar. Chem.* **2006**, *98*, 43. doi:10.1016/J.MARCHEM.2005.06.004
- [89] R. L. Siefert, A. M. Johansen, M. R. Hoffmann, S. O. Pehkonen, Measurements of trace metal (Fe, Cu, Mn, Cr) oxidation states in fog and stratus clouds. *J. Air Waste Manag. Assoc.* **1998**, *48*, 128. doi:10.1080/10473289.1998.10463659
- [90] G. Zhuang, Z. Yi, R. A. Duce, P. R. Brown, Chemistry of iron in marine aerosols. *Global Biogeochem. Cycles* **1992**, *6*, 161. doi:10.1029/92GB00756
- [91] P. Warneck, *Chemistry of the Natural Atmosphere*, 2nd edn **1999** (Academic Press: San Diego, CA).
- [92] C. D. O'Dowd, E. Becker, M. Kulmala, Mid-latitude North Atlantic aerosol characteristics in clean and polluted air. *Atmos. Res.* **2001**, *58*, 167. doi:10.1016/S0169-8095(01)00098-9
- [93] A. Ito, Global modeling study of potentially bioavailable iron input from shipboard aerosol sources to the ocean. *Global Biogeochem. Cycles* **2013**, *27*, 1. doi:10.1029/2012GB004378
- [94] N. M. Mahowald, S. Engelstaedter, C. Luo, A. Sealy, P. Artaxo, C. Benitez-Nelson, S. Bonnet, Y. Chen, P. Y. Chuang, D. D. Cohen, F. Dulac, B. Herut, A. M. Johansen, N. Kubilay, R. Losno, W. Maenhaut, A. Paytan, J. M. Prospero, L. M. Shank, R. L. Siefert, Atmospheric iron deposition: global distribution, variability, and human perturbations. *Annu. Rev. Mar. Sci.* **2009**, *1*, 245. doi:10.1146/ANNUREV.MARINE.010908.163727
- [95] F. D. Meyer-Oeste, *Method for Cooling the Troposphere. Int. Patent CA 2748680 A1 2010*.
- [96] W. C. Keene, M. Khalil, K. Aslam, D. J. Erickson, A. McCulloch, T. E. Graedel, J. M. Lobert, M. L. Aucott, S. L. Gong, D. B. Harper, G. Kleiman, P. Midgley, R. M. Moore, C. Seuzaret, W. T. Sturges, C. M. Benkovitz, V. Koropalov, L. A. Barrie, Y. F. Li, Composite global emissions of reactive chlorine from anthropogenic and natural sources: reactive chlorine emissions inventory. *J. Geophys. Res.* **1999**, *104*, 8429. doi:10.1029/1998JD100084

The estimated yearly global iron demand by the ISA method as calculated by Wittmer et al., (2015) resulted to 220 Mt/year. Meanwhile it has been revealed that this result is wrong and needs to be reduced by at least 3 orders of magnitude. Wittmer et al., (2015) used a wrong calculation bases because they particularly ignored that:

* ISA precursor iron oxide aerosol does not need to coagulate with the sea-spray particles as an chloride source because it absorbs hydrogen chloride from the gaseous phase

* According to the pyrogenic iron oxide particle diameter range of 0,01 to 0.1µm ISA particles have orders of magnitude longer life times in the atmosphere according to more than one week than the sea-spray particles Wittmer et al. used as calculation basis.

* According to the ISA particle diameter range which is about up to 2 orders smaller than calculated (the mass of the sea salt aerosol particles is concentrated in the diameter range 1 to 10µm) even the photo-reactive surface of ISA is at least 1 to more than 2 orders of magnitude higher than Wittmer calculated.

According to a later calculation (<http://www.earth-syst-dynam.net/8/1/2017>) the iron demand of the ISA method is ~0.2 Mt/year or lower. Franz Dietrich Oeste, 05.12.2018